Missouri S&T Library and Learning Resources

Scholars' Mine

Masters Theses

Student Theses and Dissertations

Summer 2016

Biodegradable electronic and optical devices toward temporary implants

Md Shihab Adnan

Follow this and additional works at: https://scholarsmine.mst.edu/masters_theses

Part of the Biomedical Engineering and Bioengineering Commons, Electrical and Computer Engineering Commons, and the Materials Science and Engineering Commons

Department:

Recommended Citation

Adnan, Md Shihab, "Biodegradable electronic and optical devices toward temporary implants" (2016). *Masters Theses*. 7864.
https://scholarsmine.mst.edu/masters_theses/7864

This thesis is brought to you by Scholars' Mine, a service of the Missouri S&T Library and Learning Resources. This work is protected by U. S. Copyright Law. Unauthorized use including reproduction for redistribution requires the permission of the copyright holder. For more information, please contact scholarsmine@mst.edu.

www.manaraa.com

BIODEGRADABLE ELECTRONIC AND OPTICAL DEVICES TOWARD TEMPORARY IMPLANTS

by

MD SHIHAB ADNAN

A THESIS

Presented to the Faculty of the Graduate School of the

MISSOURI UNIVERSITY OF SCIENCE AND TECHNOLOGY

In Partial Fulfillment of the Requirements for the Degree

MASTER OF SCIENCE IN ELECTRICAL ENGINEERING

2016

Approved by

Dr. Chang-Soo Kim

Dr. Matthew J. O'Keefe

Dr. Delbert E. Day

www.manaraa.com

© 2016

Md Shihab Adnan

All Rights Reserved

www.manaraa.com

PUBLICATION THESIS OPTION

This thesis consists of the following articles that are intended for publication as follows:

Paper I, pages 9-25 are to be submitted to IEEE Electron Device Letters.

Paper II, page 26-43 are intended for submission to IEEE Sensors Conference.

Appendices may be used as supplementary information for two publications. This thesis has been formatted according to Missouri University of Science and Technology specification.

www.manaraa.com

ABSTRACT

Implantable biomedical devices have a high potential to revolutionize health care technologies in near future. Implantable devices can be classified as permanent prosthetic devices such as pacemakers or nerve stimulants and temporary devices for intermediate monitoring and control scenario which are still in research phase. In contrast to permanent device, temporary implants lose functionality and become unnecessary after intended operational lifetime which may pose serious electromagnetic and biomedical safety concern, latent complications at the implanted sites and possible ethical issues if not removed from body by an additional surgical operation.

The first paper of this thesis focuses on exploring the feasibility of implantable inorganic bioresorbable thin film inductive devices utilizing borate glass as the substrate material. This inductive device is fully functional for a desired time inside simulated body fluid and then completely dissolves without causing any safety issues.

The second paper of the thesis demonstrates a new concept of biodegradable optical devices based on specially formulated reactive phosphate-based glass for potential theragnostic (therapy and diagnosis) applications. This work is focused on the feasibility test of biodegradable glass based light-guiding device for potential application to light-activated therapies.

These feasibility studies are expected to continue to a variety of useful sensing and actuation (e.g. temperature, pressure, flow etc.) and light guiding applications (e.g. photodynamic) which can be applied to many biomedical areas.

www.manaraa.com

ACKNOWLEDGMENTS

The work in this thesis has been solely possible with the support and guidance of my advisor, Dr. Chang Soo Kim. His direction has been invaluable and will be greatly appreciated.

I wish to my express sincere thanks to Dr. Delbert E. Day for his time deliberating on challenges, devising solutions, and his constant encouragement throughout this study. I am indebted to Dr. Matthew J. O'Keefe for his support by giving access to different lab facility and his suggestion and inspiration. I wish to express my sincere gratitude to Dr. Richard K. Brow for his support, guidance and letting me access his lab for indefinite time. His corrective suggestion and encouragement were also inspirational for conducting my research. I am thankful to Dr. Mohammad Tyeb Ghasr and Dr. Reza Zhougi for letting me use their lab. Dr. Mohammad Tyeb Ghasr also helped me by giving insightful information regarding CST, Labview and high frequency transmission line basics. I am grateful for all the help from the technical staff of Material Research Center Eric Bohannan, Ron Haas, Brian Porter and Clarissa Wisner, PhD candidate Parker Fredenberg & Jincheng Bai and undergraduate student Noor Shoaib in Materials Science and Engineering for making bioactive glass samples for the experiments and my fellow lab mates Dinesh Reddy and Devdatt Chattopadhyay for their help from time to time.

I am thankful to God for all the opportunities. I wish to express my endless gratitude to my parents, Md Obaidul Haque and Shafia Khatoon, for their moral support and encouragement. Appreciation is also extended to my spouse, Quazi Nahida Sultana, and my other friends at Missouri University of Science and Technology.

www.manaraa.com

TABLE OF CONTENTS

Page

PUBLICATION THESIS OPTION iii

ABSTRACT iv

ACKNOWLEDGEMENTS v

LIST OF ILLUSTRATIONS ix

LIST OF TABLES x

SECTION

1. INTRODUCTION 1

   1.1. CONCEPT OF BIODEGRADABLE IMPLANTS 1

   1.2. BIODEGRADABLE GLASS MATERIAL 1

   1.3. BIODEGRADABLE ELECTRONIC DEVICES FOR SENSING APPLICATIONS 2

   1.4. BIODEGRADABLE OPTICAL DEVICES FOR THERAPEUTIC APPLICATIONS 4

REFERENCES 7

PAPER

I. WATER-SOLUBLE GLASS SUBSTRATE AS A PLATFORM FOR BIODEGRADABLE SOLID-STATE DEVICES 9

   ABSTRACT 9

1. INTRODUCTION 10

2. DEVICE OPERATION CONCEPT 12

3. EXPERIMENTAL DETAILS 14

   3.1. GLASS SUBSTRATE PREPARATION 14

www.manaraa.com

3.2. DEVICE FABRICATION ……..... 14

3.3. MEASUREMENT SETUP ……..... 15

3.4. SIMULATION ……..... 16

4. RESULTS AND DISCUSSIONS …….. 17

4.1. SUBSTRATE DISSOLUTION …… 17

4.2. DC RESISTANCE AND AC IMPEDANCE ……..... 17

4.3. SCATTERING PARAMETER (S11) ……..... 19

5. CONCLUSIONS ……..... 21

REFERENCES ……..... 22

II. BIODEGRADABLE OPTICAL FIBER FOR TEMPORARY THERAPEUTIC APPLCATIONS ……..... 26

ABSTRACT ……..... 26

1. INTRODUCTION ……..... 27

2. FIBER OPERATION CONCEPT ……..... 28

3. EXPERIMENTAL DETAILS ……..... 30

3.1. FIBER PREPARATION ……..... 30

3.2. DISSOLUTION BEHAVIOR ……..... 31

3.3. OPTICAL PROPERTIES OF BULK GLASS ……..... 31

3.4. TRANSMISSION PROPERTIES OF FIBER ……..... 33

4. RESULTS AND DISCUSSIONS ……..... 35

4.1. REFRACTIVE INDEX ……..... 35

4.2. TRANSMISSION/ABSORPTION OF BULK GLASS ..…… 36

4.3. PROPAGATION LOSS OF FIBER ……..... 37

4.4. TRANSMISSION DURING DISSOLUTION …… 37

www.manaraa.com

4.5. SIMULATION ……...……..... 39

5. CONCLUSIONS ……..... 41

REFERENCES ……..... 42

SECTION

2. CONCLUSIONS ……..... 44

APPENDICES

A. PROCEDURE FOR PREPARING BORATE GLASS WAFER ……... 46

B. PROCEDURE FOR THIN OXIDE FILM COATING AND INDUCTOR PATTERNING ……..... 52

C. PROCEDURE FOR INDUCTOR PACKAGING ……..... 54

D. SIMULATED BODY FLUID (SBF) RECIPE ……..... 57

E. PROCEDURE FOR CHARACTERIZATION OF BORATE GLASS ……. 59

F. RESULTS OF BORATE GLASS CHARACTERIZATION ……..... 62

G. PROCEDURE FOR INDUCTOR CHARACTERIZATION ……..... 69

H. PROCEDURE FOR PHOSPHATE GLASS CHARACTERIZATION …… 75

I. RESULTS OF PHOSPHATE GLASS CHARACTERIZATION ……. 78

VITA ……..... 83

www.manaraa.com

LIST OF ILLUSTRATIONS

Figure Page

SECTION

1.1. Various Bioactive Glass Scaffold Structures ……. 3

PAPER I

2.1. Conceptual Device Functionality Versus Time …… 13

3.1. Cross Sectional View of Device, Simplified Model and Dissolution …….. 15

4.1. DC Resistance and AC Impedance Behavior Over Time …… 18

4.2. Scattering Parameter Response Over Time …….. 19

PAPER II

1.1. Biodegradable Fiber Operation Concept …….. 29

3.1. Conceptual Diagram Of Transmission During Dissolution …… 34

4.1. Refractive Index Of Phosphate Buffer Solution ……... 35

4.2. Transmission/Absorption …….. 37

4.3. Dissolution Behavior Of Phosphate Fiber …… 39

4.4. Transmission Change During Dissolution Of Fiber In PBS …… 40

www.manaraa.com

LIST OF TABLES

Table Page

PAPER II

3.1. Fiber Composition …….. 30

3.2. Polishing Steps …… 32

4.1. Propagation Loss ……. 38

www.manaraa.com

1. INTRODUCTION

1.1. CONCEPT OF BIODEGRADABLE IMPLANTS

There are two different categories of implantable medical devices. The first involves permanent prosthetic devices that are currently being used for rehabilitation purposes including cardiac pacemakers and nerve stimulation implants. The second category, still in an emerging concept stage, involves temporary devices for interventional medical monitoring and control scenarios. After their intended operational lifetime, the devices either lose their functionality or become unnecessary. However, these devices are left inside the body unless removed by an additional surgical operation. This may cause significant electromagnetic and/or biomechanical safety concerns, latent complications at the implanted sites, and possible ethical issues [1-3].

One critical missing link to implement these temporary systems is the realization of biodegradable (dissolvable and resorbable) devices. During their intended lifetime, the implanted biodegradable sensors are completely functional and protected from the local environment. At the end of the intended operational lifetime, the device will degrade/resorb at a rate determined by the chemical composition of the device components.

1.2. BIODEGRADABLE GLASS MATERIAL

Glass is an excellent material for the dielectric packaging layers. It has a low temperature coefficient and hysteresis, little dielectric aging, zero piezoelectric noise and low dielectric loss (i.e. dissipation factor). Fusion bonding of conventional glass wafers

www.manaraa.com

(e.g. silicate-based pyrex glass) is a common method for packaging electronic and MEMS devices [11]. Various glass frits and spin-on-glasses have been successfully used as the bonding layer between two wafers for low-temperature fusion bonding (< 400 °C) [12].

Biodegradable glasses are a class of materials that react in vivo and change their chemical composition when in contact with living tissue, allowing ingrowth of cells to become a part of the tissue itself and eventually resorbed [13]. Various three-dimensional scaffolds can be fabricated as shown in Fig. 1.1 (a) - (d). Initial applications were mostly for artificial scaffolds to repair hard tissues such as in dental and orthopedic applications. As shown in Fig. 1.1 (e), the bioactive glass exchanges ionic species with the surrounding tissue to form a porous bone-like hydroxyapatite layer.

This type of bioactive glass will serve as the main structural material for the requisite micro device proposed. Since bioactive glasses exhibit high electrical resistivity (~ giga Ω·cm at room temperature) it is possible to use them as the electric substrate and packaging material. The operational lifetime of the implanted system is controlled by changing the composition of the bioactive glass substrate and the encapsulating layer that surrounds the active device. Furthermore, some bioactive glasses are X-ray image able by their composition, which is an additional merit to monitor the shape of device during the course of biodegradation process.

1.3. BIODEGRADABLE ELECTRONIC DEVICES FOR SENSING APPLICATIONS

This thesis is devoted to the fabrication of biodegradable solid-state devices using biodegradable glass materials as the active device components, thus creating a new class

www.manaraa.com

of biomedical device platforms with capabilities that cannot be matched by devices that rely on organic materials. Biodegradable platforms can serve as fully implanted systems deep inside the body to monitor physical/chemical parameters in internal organs and circulatory tracts.

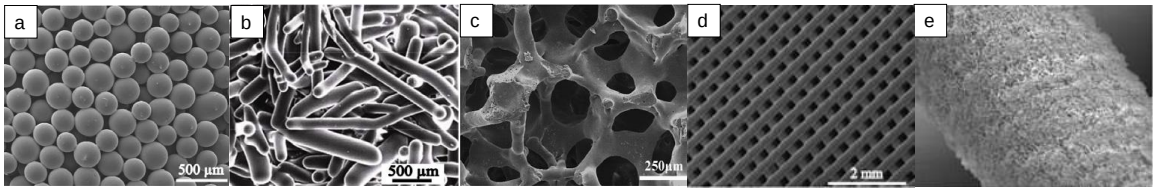

Figure 1.1. Various Bioactive Glass Scaffold Structures. Fabricated by (a) thermal bonding of microspheres, (b) thermal bonding of short microfibers, (c) polymer foam replication and (d) micro-grid robocasting. (e) Bioactive glass fiber reacts in a body fluid and converts to bone-like material (hydroxyapatite) with a highly porous surface. [13].

One of the most important capabilities in the biomedical areas is the continuous pressure monitoring with minimal human intervention in numerous areas. The most straightforward method of delivering power and communicating data with implanted devices is the wireless approach. One configuration that can take full advantage of our biodegradable device platform is the wireless L-C (inductor-capacitor) resonant sensor that does not need active peripheral circuits. This method was demonstrated to be promising in monitoring the intraocular eye pressure [14-15] and cardiac artery pressure when combined with metal stents [16-17].

The two most important parameters in this configuration are the resonant frequency, f (i.e. location of impedance peak) and the quality factor, Q (Q-factor) of the

www.manaraa.com

coupled system (i.e. peak sharpness):

$$f = 1/[2\pi(LC)^{1/2}] \text{ and } Q = (L/C)^{1/2}/R_p \quad (1)$$

Here, L, C and R_p are the inductance, capacitance (i.e. pressure-sensitive element) and parasitic resistance of the sensor. The change in pressure can be quantified in terms of the shift of the resonant frequency f as the capacitance changes. In this thesis, only the inductor is demonstrated for these wireless circuit elements with biodegradable materials to produce a biodegradable device.

1.4. BIODEGRADABLE OPTICAL DEVICES FOR THERAPEUTIC APPLICATIONS

Photodynamic therapy (PDT) is an emerging therapeutic modality for cancers and infective diseases based on the light-induced cell death [18-19]. Light-activated reactive oxygen species (ROS) destroys the tissue with three required ingredients which are light (mostly visible range), oxygen dependent photosensitizer (mostly porphyrin-based) and tissue oxygen. This approach is particularly promising because of the use of non-ionizing radiation (visible to near IR), minimally invasive in nature, highly portable and low cost procedure. However there are several challenging technical issues are there for PDT to become mainstream cancer treatment, including a limitation to surface treatment, highest possible single dose of light and photosensitizer per outpatient visit (as opposed to low dose repetitive interventional therapy) and low efficiency for large solid tumors with hypoxic environment owing to oxygen unavailability.

This thesis focuses on a new area that can benefit the most from biodegradable devices in the patient-specific-closed loop PDT cancer therapy over an extended time

www.manaraa.com

frame (~months to year). The indicated limitations can be overcome by using a light guiding device that is biocompatible in nature. This approach has been identified as a new direction in PDT development which focuses on delivering the optimal light and photosensitizer continuously over days especially for brain tumors for which this therapeutic modality is more efficient appropriate [20-21].

Biodegradable light-guiding devices (e.g. optical fibers) can deliver localized optimal dose of light to deep locations (~several inches). Although interstitial illumination with laparoscopes is conducted as an intraoperative adjuvant treatment, it is mostly limited to single therapy that requires repeated surgeries if the cancer recurs. In contrast to interstitial illumination, implantable biodegradable optical fibers with percutaneous couplers can serve long time monitoring and perform necessary therapeutic procedures with appropriate structure during the intended lifetime. The biodegradable fibers will not have any concern for surgical operation for removal. In addition to this, biodegradable hollow fiber can be formed to deliver photosensitizer and oxygen while acting as light guiding device.

Furthermore monitoring the oxygen level within tumor tissue is one of the core parameters of explicit dosimetry during the PDT to evaluate the effectiveness of therapy [22] which can be achieved by luminescence quenching effect detection caused by oxygen level with appropriate device structure.

In this thesis, bioactive phosphate-based glass has been chosen to form biodegradable fibers due to its high refractive index, proper mechanical strength and flexibility.

www.manaraa.com

The lifetime of this fibers are easily manipulable by changing the composition. This fiber is expected to be completely degradable inside body leaving minimum trace after the therapy is completed during the intended operational lifetime.

www.manaraa.com

REFERENCES

[1] W. Irnich, "Electronic security systems and active implantable medical devices," Pacing and clinical electrophysiology, vol. 25, pp. 1235-1258, 2002.

[2] K. R. Foster and J. Jaeger, "Ethical implications of implantable radiofrequency identification (RFID) tags in humans," The American Journal of Bioethics, vol. 8, pp. 44-48, 2008.

[3] E. Neufeld, S. Kühn, G. Szekely, and N. Kuster, "Measurement, simulation and uncertainty assessment of implant heating during MRI," Physics in medicine and biology, vol. 54, p. 4151, 2009.

[4] M. Peuster, P. Beerbaum, F.-W. Bach, and H. Hauser, "Are resorbable implants about to become a reality?," Cardiology in the Young, vol. 16, pp. 107-116, 2006.

[5] M. Zilberman and R. C. Eberhart, "Drug-eluting bioresorbable stents for various applications," Annu. Rev. Biomed. Eng., vol. 8, pp. 153-180, 2006.

[6] M. Moravej and D. Mantovani, "Biodegradable metals for cardiovascular stent application: interests and new opportunities," International journal of molecular sciences, vol. 12, pp. 4250-4270, 2011.

[7] D.-H. Kim, Y.-S. Kim, J. Amsden, B. Panilaitis, D. L. Kaplan, F. G. Omenetto, et al., "Silicon electronics on silk as a path to bioresorbable, implantable devices," Applied physics letters, vol. 95, p. 133701, 2009.

[8] C. J. Bettinger and Z. Bao, "Organic Thin-Film Transistors Fabricated on Resorbable Biomaterial Substrates," Advanced materials, vol. 22, pp. 651-655, 2010.

[9] M. Irimia-Vladu, P. A. Troshin, M. Reisinger, L. Shmygleva, Y. Kanbur, G. Schwabegger, et al., "Biocompatible and Biodegradable Materials for Organic Field-Effect Transistors," Advanced Functional Materials, vol. 20, pp. 4069-4076, 2010.

[10] S.-W. Hwang, H. Tao, D.-H. Kim, H. Cheng, J.-K. Song, E. Rill, et al., "A Physically Transient Form of Silicon Electronics," Science, vol. 337, pp. 1640-1644, 2012-09-28 00:00:00 2012.

[11] P. Lindner, V. Dragoi, S. Farrens, T. Glinsner, and P. Hangweier, "Advanced techniques for 3D devices in wafer-bonding processes," Solid State Technology, vol. 47, pp. 55-58, 2004.

www.manaraa.com

[12] P. Ramm, J. J.-Q. Lu, and M. M. Taklo, Handbook of Wafer Bonding: John Wiley & Sons, 2012.

[13] M. N. Rahaman, D. E. Day, B. Sonny Bal, Q. Fu, S. B. Jung, L. F. Bonewald, et al., "Bioactive glass in tissue engineering," Acta Biomaterialia, vol. 7, pp. 2355-2373, 6// 2011.

[14] J. Coosemans, M. Catrysse, and R. Puers, "A readout circuit for an intra-ocular pressure sensor," Sensors and Actuators A: Physical, vol. 110, pp. 432-438, 2004.

[15] P.-J. Chen, D. C. Rodger, S. Saati, M. S. Humayun, and Y.-C. Tai, "Microfabricated implantable parylene-based wireless passive intraocular pressure sensors," Microelectromechanical Systems, Journal of, vol. 17, pp. 1342-1351, 2008.

[16] K. Takahata, Y. B. Gianchandani, and K. D. Wise, "Micromachined antenna stents and cuffs for monitoring intraluminal pressure and flow," Microelectromechanical Systems, Journal of, vol. 15, pp. 1289-1298, 2006.

[17] E. Y. Chow, A. L. Chlebowski, S. Chakraborty, W. J. Chappell, and P. P. Irazoqui, "Fully wireless implantable cardiovascular pressure monitor integrated with a medical stent," Biomedical Engineering, IEEE Transactions on, vol. 57, pp. 1487-1496, 2010.

[18] D. E. J. G. J. Dolmans, D. Fukumura, and R. K. Jain, "Photodynamic therapy for cancer," Nat Rev Cancer, vol. 3, pp. 380-387, 05//print 2003.

[19] T. J. Dougherty, C. J. Gomer, B. W. Henderson, G. Jori, D. Kessel, M. Korbelik, et al., "Photodynamic therapy," J Natl Cancer Inst, vol. 90, pp. 889-905, Jun 17 1998.

[20] S. K. Bisland, L. Lilge, A. Lin, R. Rusnov, and B. C. Wilson, "Metronomic photodynamic therapy as a new paradigm for photodynamic therapy: rationale and preclinical evaluation of technical feasibility for treating malignant brain tumors," Photochem Photobiol, vol. 80, pp. 22-30, Jul-Aug 2004.

[21] B. C. Wilson, S. K. Bisland, A. Bogaards, A. Lin, E. H. Moriyama, K. Zhang, et al., "Metronomic photodynamic therapy (mPDT): concepts and technical feasibility in brain tumor," in Biomedical Optics 2003, 2003, pp. 23-31.

[22] Z. Huang, H. Xu, A. D. Meyers, A. I. Musani, L. Wang, R. Tagg, et al., "Photodynamic therapy for treatment of solid tumors--potential and technical challenges," Technol Cancer Res Treat, vol. 7, pp. 309-20, Aug 2008.

www.manaraa.com

PAPER

I. WATER-SOLUBLE GLASS SUBSTRATE AS A PLATFORM FOR BIODEGRADABLE SOLID-STATE DEVICES

ABSTRACT

A biodegradable glass material is utilized as a novel functional element of solid-state devices. A glass substrate serves as the structural platform on which thin film spiral devices are built. Intentional failure of the device as a result of rapid structural disintegration in saline solution is demonstrated in DC, AC and RF ranges that agree well with simulation.

Index Terms – biodegradation, bioactive glass, RLC, resonance

www.manaraa.com

1. INTRODUCTION

Biodegradable devices are in the emerging concept stage, involving temporary implanted devices with limited lifetime. The devices are to be fully functional during an intended operational lifetime after which they lose functionality via dissolution and resorption. A wide range of biomedical applications that can potentially benefit from short-term implants was reviewed extensively [1]. An increasing need for biodegradable devices has been addressed in the literature, focusing on passive devices including metal or polymer stents [2-3].

Accordingly, the concepts of active biodegradable devices including electronics and sensors have been demonstrated [5-11]. These devices are composed of organic materials (e.g. biodegradable polymers) and biodegradable metals/semi-conductors. Typically, the organic elements serve as the structural substrates and insulation layers for biodegradation, except in one case that used metal foils [12]. Organic materials are degraded by bulk hydration that continuously changes the original bulk properties during degradation. Retaining the structural integrity of substrates and the insulating property of insulation layers is critically important to maintain the device reliability during intended use [12-15]. Inorganic materials are superior in this respect since the hydrolysis occurs only at the surface, allowing the retention of bulk mechanical, thermal and chemical properties until those elements are largely consumed.

We report a new approach that uses biodegradable glasses as the substrate. The aim is to prepare devices compatible with traditional solid-state processes to function reliably during lifetime followed by a rapid failure. These glasses, normally known as

www.manaraa.com

bioactive glasses, are a class of biomaterials commonly used in tissue engineering that react with surrounding tissue to become a part of the tissue itself and eventually absorbed [16-17]. Their reaction rates can be controlled with their compositions ranging from fast (e.g. ~ mm/day with borate- and phosphate-based) to extremely low rate (e.g. ~ nm/day with silicate-based) [18-20]. Simple thin film devices were prepared on the glass substrates to demonstrate the device behavior in various frequency ranges during the course of structural degradation in solution.

www.manaraa.com

2. DEVICE OPERATION CONCEPT

Fig. 2.1. shows the expected behavior of the device exposed to body fluids. The major portion of the substrate is made of a fast reacting glass material. The bottom layer is a slowly reacting glass film. It is consumed during a presumed lifetime (i.e. A to B stage) with the active device being fully functional due to its top insulation layer. The lifetime can be manipulated by adjusting the compositions and thickness of the bottom layer. The dissolution of the entire glass substrate occurs rapidly once exposed to solution, leaving only a top layer. This crust layer is expected to structurally disintegrate without mechanical support. It is critically important to design the duration of failure (i.e. B to D stage) as short as possible to prevent false results and safety concerns caused by continued use.

Common silicon-based films (e.g. SiO_2 and Si_3N_4) can serve as the top insulation layer since these have been used extensively for insulating liquid sensors including ion-sensitive field-effect transistors [21]. Silicon-based biodegradable devices were first suggested by Canham *et al*. [22-23]. Although the dissolution rates are slow, the fragments of silicon-based crust layer eventually decompose to silicic acid to become a metabolite or excreted from body. Therefore, it is highly feasible to implement silicon-based biodegradable devices having proper form factors (i.e. large surface-to-volume ratio) as demonstrated by porous silicon drug delivery vehicles [24] and silicon-based biodegradable electronics [8,12,14,25].

www.manaraa.com

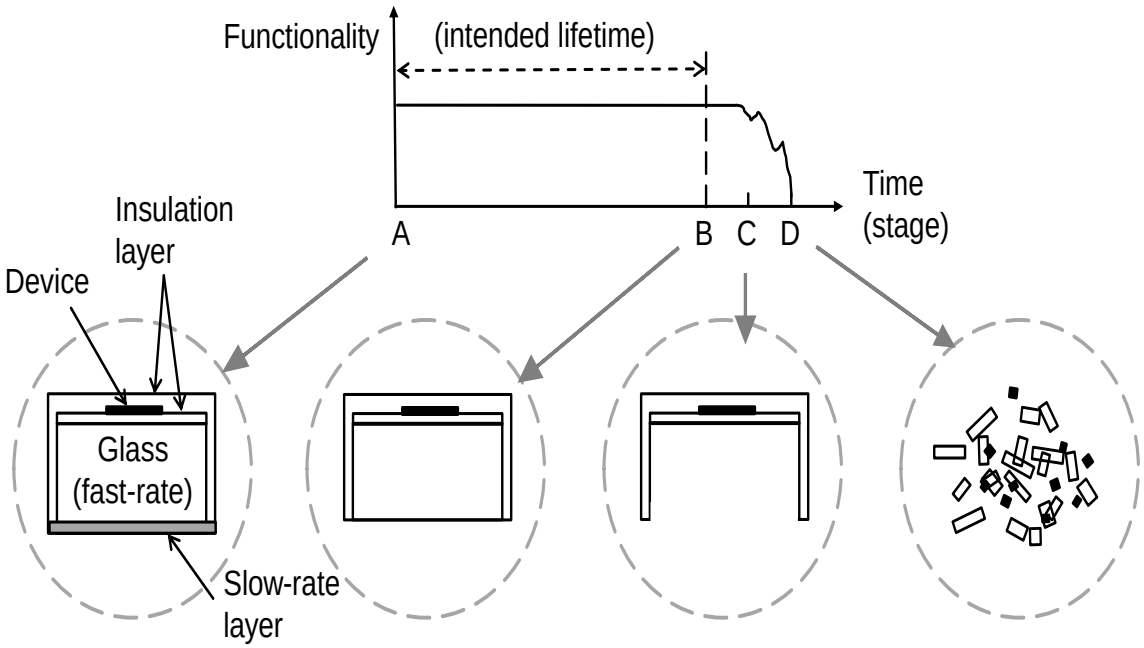

Figure 2.1. Conceptual Device Functionality Versus Time. Rapid failure after the intended operational lifetime: initial structure (stage A), dissolution of slow-rate glass film (e.g. several months) (stage B), dissolution of fast-rate glass substrate (e.g. 1-2 days) (stage C) and physical disintegration of crust insulation and device layers (stage D).

www.manaraa.com

3. EXPERIMENTAL DETAILS

3.1. GLASS SUBSTRATE PREPARATION

The glass substrates were manually prepared. Borate glass was prepared by melting sodium tetraborate (12305, anhydrous 99.5%, Alfa Aesar) in a platinum crucible at 1,000 ^{o} C for 30 minutes. The melt was poured into a stainless steel cylindrical mold and annealed at 450 ^{o} C for 30 minutes to form a glass rod (14 mm diameter, 30 mm). Sliced circular substrates were mounted on aluminum holders and ground using silicon carbide foils (180 to 1200 grit sizes, Struers) followed by polishing with a diamond media (DP spray P, Struers). The final surface roughness was approximately 0.25 um measured by atomic force microscopy (Nanoscope IIIa, Digital Instrument).

3.2. DEVICE FABRICATION

The prototype device in Fig. 3.1.(a) without the slow rate layer is intended to demonstrate the B to D stage in Fig. 2.1. The top and side surfaces of the glass substrates were coated with a silicon dioxide (SiO_2) blanket insulation layer (1 um thick) by sputtering (Discover 18, Denton Vacuum). A spiral coil device (2.4 mm diameter, 0.2 mm line width, 0.15 mm line spacing) was fabricated with a gold layer (120 nm thick) deposited by sputtering (Bio-Rad E5400 flash coater) and patterned using a stainless steel shadow mask (4 mil thick). An SMA RF connector (0731000115, Molex) was connected to the device with silver paste (Z04969, SPI). The entire SMA connector was encapsulated in silicone (3140, Corning). A nylon washer (11 mm inner diameter, 0.5 mm thick) was glued at the bottom surface with silicone to ensure a fixed exposed area.

www.manaraa.com

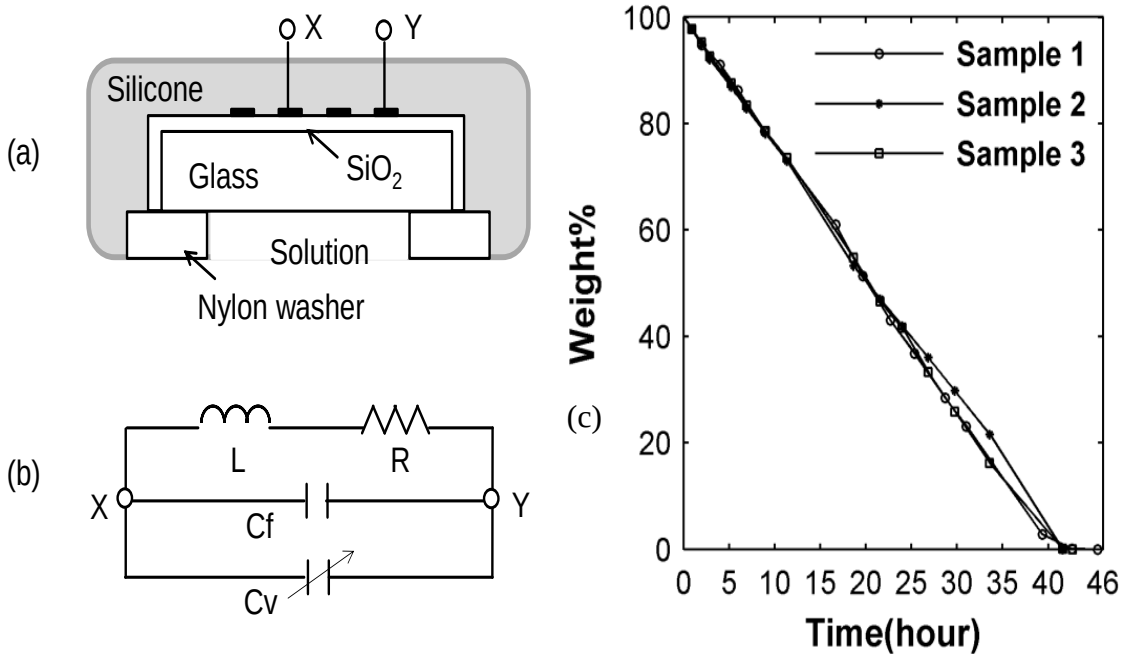

Figure 3.1. Cross Sectional View of Device, Simplified Model and Dissolution. (a) Cross-sectional view of the spiral thin film device after encapsulation to demonstrate the stage B to D in Fig. 1. (b) Simplified model of the device (L: inductance of spiral film, R: series resistance along spiral film, C_F: fixed capacitance through SiO_2 and silicone; C_V: variable capacitance through glass and solution). Au film can be replaced with biodegradable film (e.g. Ag, Mg) for actual applications. (c) Dissolution behavior of bare glass substrates (2.7 mm thick, 14 mm diameter, no coating/encapsulation) in a simulated body fluid (SBF) solution (pH 7.4 at 37 ^{o}C).

3.3. MEASUREMENT SETUP

All dissolution tests were conducted in a simulated body fluid (SBF) solution (pH 7.4) [26]. The device was submerged in a 1 L solution placed in an incubator (Heratherm, Thermo Scientific) at 37 ^{o} C and tested for dissolution behavior. For monitoring the change in DC and AC impedance levels during dissolution, the device was connected to an electrochemical potentiostat (Femtostat, Gamry). The scattering parameter (S11) was monitored in an RF frequency range with a vector network analyzer (VNA) (E8753, Agilent). A 12-inch 50 ohm cable was connected to extend the connectivity up to the

www.manaraa.com

VNA. Since the VNA was calibrated only at the port while the device was present after the cable, the 1-port 3-term error model [27] was used to obtain the actual response of the device.

3.4. SIMULATION

Microwave studio (Computer Simulation Technology) was used to simulate the resonance behavior of the RLC model shown in Fig. 3.1. (b). Inductance L was calculated by a data fitted monomial expression [28], whereas series resistance R was measured with a multi-meter. Complex dielectric constants of the glass and solution were calculated from S11 parameter using waveguide method with the same VNA [29]. Dielectric properties of SiO_2 and silicone were taken from literature [30-31]. Utilizing these values, two parasitic capacitive elements, C_F and C_V, were calculated by a known method [32]. The calculated resonance frequency was 2.1 GHz similar to the range of other biodegradable resonance devices [5,8,10].

www.manaraa.com

4. RESULTS AND DISCUSSIONS

4.1. SUBSTRATE DISSOLUTION

Fig. 3.1.(c) shows the rapid weight loss during the course of dissolution of bare glass substrates without any coated layer. The linear loss rate is approximately 5.5 mg/hour with an initial surface area of 4.35 cm^2. As expected, this rate is moderately higher than those of the borate glasses containing silicates [18,20]. Fig. 3.1.(c) represents the rapid failure after a presumed lifetime (i.e. t = 0 hour being the onset of stage B in Fig.1.) since the bare substrates has no protective slow-rate layer. Although each substrate prepared manually was used as a single "dice" at this phase, it is expected that large diameter "wafers" can be mass-produced by a refined manufacturing procedure. Therefore, the biodegradable glass substrate is considered as an excellent candidate that maintains the structural integrity to support the devices during use followed by a rapid disintegration.

4.2. DC RESISTANCE AND AC IMPEDANCE

Changes in DC resistance and AC impedance of the devices were measured during substrate dissolution. Fig. 4.1. shows that both DC and AC values stay at a certain range followed by a steep decrease after one day. This change clearly demonstrated the expected behavior of rapid failure. Once the significant glass portion was consumed, the device collapsed and eventually short-circuited through the conductive solution. As expected, the device is largely resistive at this frequency range evidenced by the negligible contribution of reactive elements by comparing the DC and AC levels.

www.manaraa.com

Although a simple metal thin film device is demonstrated in this proof-of-concept stage, silicon-based devices can be implemented to be biodegradable. Traditional substrates (e.g. single crystal silicon, pyrex glass) are not appropriate for this application due to their extremely low dissolution rate. One practical approach is the silicon-on-insulator (SOI) structure [33] of the glass substrate and a thin silicon layer. Therefore, biodegradable electronics with higher electron mobility are anticipated that can cover a wider bandwidth than that of biodegradable polymer devices.

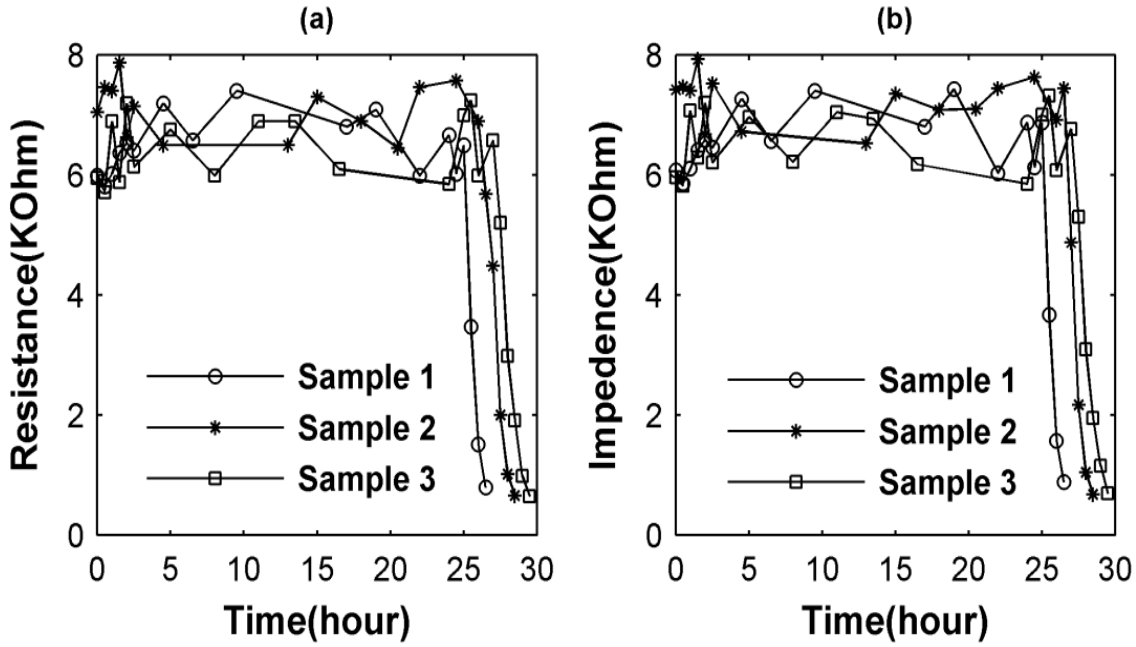

Figure 4.1. DC Resistance and AC Impedance Behavior Over Time. Temporal change of (a) DC resistance (with 0.1 V) and (b) AC impedance (with 0.1 V_{RMS}, 1 kHz) of spiral thin film devices during the dissolution of glass substrate (2.2 mm thick, 14 mm diameter). This demonstrates the device performance during the stage B - D in Fig. 2.1. (at 37 ^{o} C).

www.manaraa.com

4.3. SCATTERING PARAMETER (S11)

Fig. 4.2.(a) shows the temporal change of the S11 parameter. Upon reaching the presumable lifetime (i.e. t = 0 hour), the resonant peak started to shift toward the lower frequency side and become negligible (i.e. less than -5 dB) after a day. The shifting of the resonance was a result of increasing parasitic capacitance through the glass substrate (C_v) that was being replaced with the capacitance through the solution with a higher real dielectric constant. In addition, this rich electrolytic solution was a lossy medium that lowered the resonance peak magnitude.

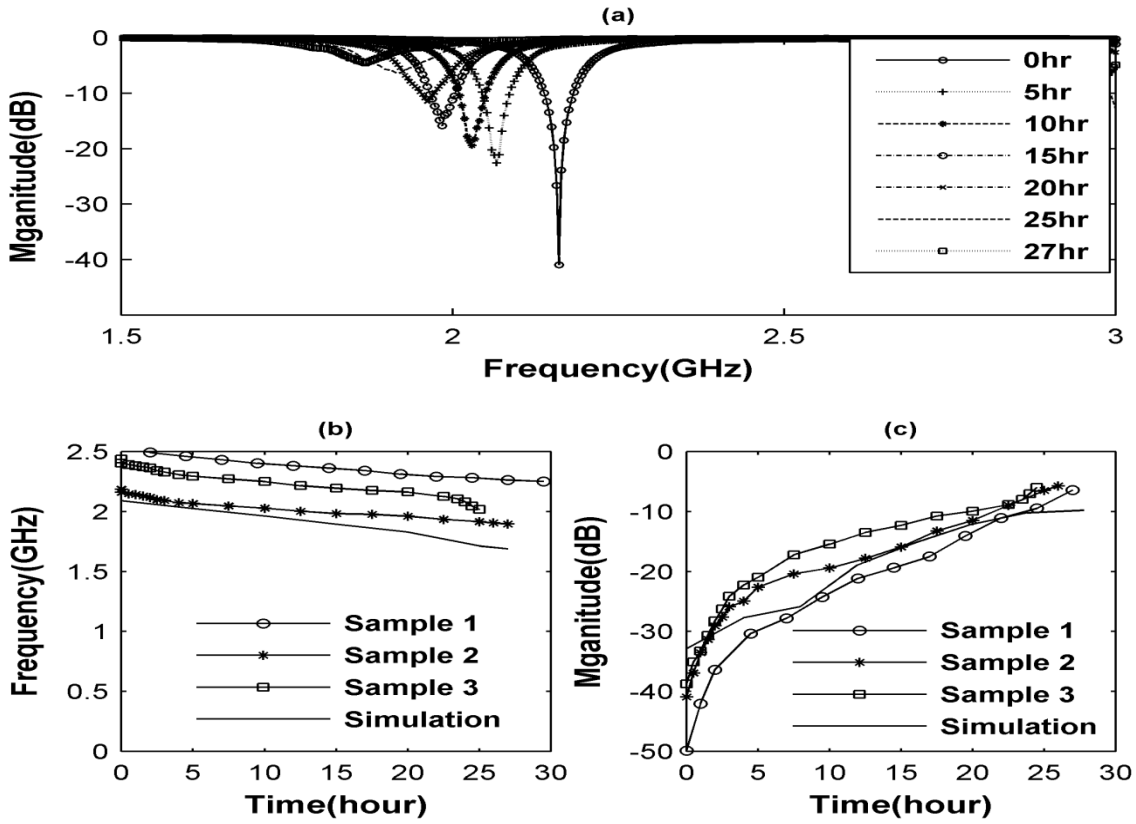

Figure 4.2. Scattering Parameter Response Over Time. Temporal change of resonance behavior of spiral thin film devices over the course of substrate dissolution (2.2 mm thick, 14 mm diameter): (a) Scattering parameter (S11) spectrum, (b) Resonant frequency and (c) Peak magnitude. This represents the stage of B - D in Fig. 1.

www.manaraa.com

The variation in resonance frequency and peak magnitude is plotted in Figs. 4.2.(b) and (c) with respect to time. A simulation was conducted based on the varying volume of glass estimated from the weight loss observation. Both experimental and simulation data show a similar trend and agree well taking into account discrepancies originated from the simplicity of model and the variations in the device preparation.

The resonance frequency of the reported device can be easily manipulated with varying spiral designs and the size of the substrate depending on future needs. Operating frequencies of implantable devices can range from kHz to several GHz range, depending on various factors including transmission distances, implanted depths, transmitter/receiver sizes and applications (e.g. signal transmission, power delivery, and thermal therapy). In this report, tests were done in a broad frequency range to explore the feasibility of various application scenarios including simple DC (e.g. device bias), low frequency (e.g. sensing) and high frequency (e.g. RF transmission).

www.manaraa.com

5. CONCLUSION

The rapid failure of device functionality (i.e. in one day after presumed lifetime) built on biodegradable glass substrates was demonstrated over a wide frequency range, which is in good agreement with simulation based on a simple model. The inorganic biodegradable substrates are more compatible with traditional device processes than other types of biodegradable substrates. It is expected to sustain the structural integrity without compromise in device reliability during operation followed by a rapid disintegration. Therefore, the use of water-soluble glasses is expected to be a viable approach to develop reliable biodegradable devices and systems.

www.manaraa.com

REFERENCES

[1] R. A. M. Receveur, F. W. Lindemans, and N. F. De Rooij, "Microsystem technologies for implantable applications," *Journal of Micromechanics and Microengineering*, vol. 17, no. 5, p. R50, Apr. 2007. DOI: 10.1088/0960-1317/17/5/R02.

[2] M. Peuster, P. Beerbaum, F. W. Bach, and H. Hauser, "Are resorbable implants about to become a reality?," *Cardiol Young*, vol. 16, no. 2, pp. 107-16, Apr. 2006. DOI: 10.1017/S1047951106000011.

[3] M. Zilberman and R. C. Eberhart, "Drug-eluting bioresorbable stents for various applications," *Annu Rev Biomed Eng*, vol. 8, pp. 153-80, Jul. 2006. DOI: 10.1146/ANNUREV.BIOENG.8.013106.151418.

[4] H. Hermawan, D. Dubé, and D. Mantovani, "Developments in metallic biodegradable stents," *Acta Biomaterialia*, vol. 6, no. 5, pp. 1693-1697, May 2010. DOI: http://dx.doi.org/10.1016/j.actbio.2009.10.006.

[5] D.-H. Kim, Y.-S. Kim, J. Amsden, B. Panilaitis, D. L. Kaplan, F. G. Omenetto, M. R. Zakin, and J. A. Rogers, "Silicon electronics on silk as a path to bioresorbable, implantable devices, " *Appl. Phys. Lett.*, vol. 95, no. 13, p. 133701, Sep. 2009.DOI: http://dx.doi.org/10.1063/1.3238552.

[6] C. J. Bettinger and Z. Bao, "Organic Thin Film Transistors Fabricated on Resorbable Biomaterial Substrates," *Advanced materials (Deerfield Beach, Fla.)*, vol. 22, no. 5, pp. 651-655, Feb. 2010. DOI: 10.1002/ADMA.200902322.

[7] M. Irimia-Vladu, P. A. Troshin, M. Reisinger, L. Shmygleva, Y. Kanbur, G. Schwabegger, M. Bodea, R. Schwödiauer, A. Mumyatov, J. W. Fergus, V. F. Razumov, H. Sitter, N. S. Sariciftci, and S. Bauer, "Biocompatible and Biodegradable Materials for Organic Field-Effect Transistors, " *Adv. Funct. Mater.*, vol. 20, no. 23, pp. 4069–4076, Sep. 2010. DOI: 10.1002/ADFM.201001031.

[8] S.-W. Hwang, H. Tao, D.-H. Kim, H. Cheng, J.-K. Song, E. Rill, M. A. Brenckle, B. Panilaitis, S. M. Won, Y.-S. Kim, Y. M. Song, K. J. Yu, A. Ameen, R. Li, Y. Su, M. Yang, D. L. Kaplan, M. R. Zakin, M. J. Slepian, Y. Huang, F. G. Omenetto, and J. A. Rogers, "A Physically Transient Form of Silicon Electronics, " *Science*, vol. 337, no. 6102, pp. 1640–1644, Sep. 2012. DOI: 10.1126/SCIENCE.1226325.

www.manaraa.com

[9] H. Tao, M. A. Brenckle, M. Yang, J. Zhang, M. Liu, S. M. Siebert, R. D. Averitt, M. S. Mannoor, M. C. McAlpine, J. A. Rogers, D. L. Kaplan, and F. G. Omenetto, "Silk-Based Conformal, Adhesive, Edible Food Sensors," *Adv. Mater.*, vol. 24, no. 8, pp. 1067–1072, Jan. 2012. DOI: 10.1002/ADMA.201103814.

[10] C. M. Boutry, H. Chandrahalim, P. Streit, M. Schinhammer, A. C. Hänzi, and C. Hierold, "Characterization of miniaturized RLC resonators made of biodegradable materials for wireless implant applications," *Sensors and Actuators A: Physical*, vol. 189, pp. 344-355, Jan. 2013. DOI:http://dx.doi.org/10.1016/j.sna.2012.08.039.

[11] L. Mengdi, A. W. Martinez, S. Chao, F. Herrault, and M. G. Allen, "A Microfabricated Wireless RF Pressure Sensor Made Completely of Biodegradable Materials, " *J. Microelectromechanical Syst.*, vol. 23, no. 1, pp. 4–13, Feb. 2014. DOI: 10.1109/JMEMS.2013.2290111.

[12] S.-K. Kang, S.-W. Hwang, S. Yu, J.-H. Seo, E. A. Corbin, J. Shin, D. S. Wie, R. Bashir, Z. Ma, and J. A. Rogers, "Biodegradable Thin Metal Foils and Spin-On Glass Materials for Transient Electronics, " *Adv. Funct. Mater.*, vol. 25, no. 12, pp. 1789–1797, Jan. 2015. DOI: 10.1002/ADFM.201403469.

[13] R. Li, H. Cheng, Y. Su, S. Hwang, L. Yin, H. Tao, M. A. Brenckle, D. Kim, F. G. Omenetto, and J. A. Rogers, "An analytical model of reactive diffusion for transient electronics, " *Adv. Funct. Mater.*, vol. 23, no. 24, pp. 3106–3114, Jun. 2013. DOI: 10.1002/ADFM.201203088.

[14] S. Kang, S. Hwang, H. Cheng, S. Yu, B. H. Kim, J. Kim, Y. Huang, and J. A. Rogers, "Dissolution behaviors and applications of silicon oxides and nitrides in transient electronics, " *Adv. Funct. Mater.*, vol. 24, no. 28, pp. 4427–4434, Jul. 2014. DOI: 10.1002/ADFM.201304293.

[15] M. A. Brenckle, H. Cheng, S. Hwang, H. Tao, M. Paquette, D. L. Kaplan, J. A. Rogers, Y. Huang, and F. G. Omenetto, "Modulated Degradation of Transient Electronic Devices through Multilayer Silk Fibroin Pockets, " *ACS Appl. Mater. Interfaces*, vol. 7, no. 36, pp. 19870–19875, Sep. 2015. DOI: 10.1021/ACSAMI.5B06059.

[16] M. N. Rahaman, D. E. Day, B. Sonny Bal, Q. Fu, S. B. Jung, L. F. Bonewald, and A. P. Tomsia, "Bioactive glass in tissue engineering, " *Acta Biomater.*, vol. 7, no. 6, pp. 2355–2373, Jun. 2011. DOI: 10.1016/J.ACTBIO.2011.03.016.

[17] L. Hench, J. W. Hench, and D. Greenspan, "Bioglass: a short history and bibliography," *Journal of the Australasian Ceramic Society*, vol. 40, no. 1, pp. 1-42, 2004.

www.manaraa.com

[18] W. Liang, C. Rüssel, D. E. Day, and G. Völksch, "Bioactive comparison of a borate, phosphate and silicate glass," *Journal of materials research*, vol. 21, no. 1, pp. 125-131, Jan. 2006. DOI: 10.1557/JMR.2006.0025.

[19] M. N. Rahaman, D. E. Day, and W. H. Huang, "Conversion of borate glass to biocompatible phosphates in aqueous phosphate solution, " in *Developments in Porous, Biological and Geopolymer Ceramics: Ceramic Engineering and Science Proceedings*, Hoboken, NJ, USA, John Wiley., 2007, Volume 28, Issue 9, pp. 171–181. DOI: 10.1002/9780470339749.CH17.

[20] S. B. Jung and D. E. Day, "Conversion kinetics of silicate, borosilicate, and borate bioactive glasses to hydroxyapatite," *Physics and Chemistry of Glasses-European Journal of Glass Science and Technology Part B*, vol. 50, no. 2, pp. 85-88, Apr. 2009.

[21] P. Bergveld, "Thirty years of ISFETOLOGY: What happened in the past 30 years and what may happen in the next 30 years, " *Sensors Actuators B Chem.*, vol. 88, no. 1, pp. 1–20, Jan. 2003.
DOI: http://dx.doi.org/10.1016/S0925-4005(02)00301-5.

[22] L. T. Canham, "Bioactive silicon structure fabrication through nanoetching techniques," *Advanced Materials*, vol. 7, no. 12, pp. 1033-1037, Dec. 1995. DOI: 10.1002/ADMA.19950071215.

[23] L. T. Canham, C. L. Reeves, D. O. King, P. J. Branfield, J. G. Crabb, and M. C. Ward, "Bioactive polycrystalline silicon," *Advanced Materials*, vol. 8, no. 10, pp. 850-852, Oct. 1996. DOI: 10.1002/ADMA.19960081020.

[24] E. J. Anglin, L. Cheng, W. R. Freeman, and M. J. Sailor, "Porous silicon in drug delivery devices and materials," *Advanced drug delivery reviews*, vol. 60, no. 11, pp. 1266-1277, Apr. 2008. DOI: 10.1016/J.ADDR.2008.03.017.

[25] S.-W. Hwang, G. Park, C. Edwards, E. A. Corbin, S.-K. Kang, H. Cheng, J.-K. Song, J.-H. Kim, S. Yu, and J. Ng, "Dissolution chemistry and biocompatibility of single-crystalline silicon nanomembranes and associated materials for transient electronics, " *ACS Nano*, vol. 8, no. 6, pp. 5843–5851, Mar. 2014. DOI: 10.1021/NN500847G.

[26] T. Kokubo, H. Kushitani, S. Sakka, T. Kitsugi, and T. Yamamuro, "Solutions able to reproduce in vivo surface-structure changes in bioactive glass-ceramic A-W3," *Journal of Biomedical Materials Research*, vol. 24, no. 6, pp. 721-734, Jun. 1990. DOI: 10.1002/JBM.820240607.

[27] S. Rehnmark, "On the Calibration Process of Automatic Network Analyzer Systems," *IEEE Trans. Microw. Theory Tech.*, vol. 22, no. 4, pp. 457–458, Apr. 1974. DOI: 10.1109/TMTT.1974.1128250.

www.manaraa.com

[28] S. S. Mohan, M. del Mar Hershenson, S. P. Boyd, and T. H. Lee, "Simple accurate expressions for planar spiral inductances," *Solid-State Circuits, IEEE Journal of*, vol. 34, no. 10, pp. 1419-1424, Oct. 1999. DOI: 10.1109/4.792620.

[29] M. T. Ghasr, D. Simms, and R. Zoughi, "Multimodal Solution for a Waveguide Radiating Into Multilayered Structures-Dielectric Property and Thickness Evaluation," *IEEE Transactions on Instrumentation and Measurement*, vol. 58, no. 5, pp. 1505-1513, Apr. 2009. DOI: 10.1109/TIM.2008.2009133.

[30] J. J. Senkevich and S. B. Desu, "Poly (tetraflouro-p-xylylene), a low dielectric constant chemical vapor polymerized polymer," *Applied physics letters*, vol. 72, no. 2, pp. 258-260, Jan. 1998. DOI: 10.1063/1.120703.

[31] J. Cervantes, R. Zárraga, and C. Salazar-Hernández, "Organotin catalysts in organosilicon chemistry," *Applied Organometallic Chemistry*, vol. 26, no. 4, pp. 157-163, Apr, 2012. DOI: 10.1002/AOC.2832.

[32] C. P. Yue and S. S. Wong, "Physical modeling of spiral inductors on silicon," *IEEE Transactions Electron Devices*, vol. 47, no. 3, pp. 560-568, Mar. 2000. DOI: 10.1109/16.824729.

[33] S. B. Jung, "Bioactive Borate Glasses," in *Bio-Glasses: An Introduction*, Chichester, UK, John Wiley., 2012, pp. 75–95. DOI: 10.1002/9781118346457.CH6.

www.manaraa.com

II. BIODEGRADABLE OPTICAL FIBER FOR TEMPORARY THERAPEUTIC APPLICATIONS

ABSTRACT

A new concept of biodegradable optical devices for therapeutic applications is exploited with a biodegradable glass material. A specially formulated phosphate-based reactive glass served as the core material of an optical fiber. Device performance demonstrates viability for delivering the light for a certain operational lifetime before structural disintegration happens in body saline, which is in well accordance with the simulation. Potential applications include the photodynamic therapy (PDT) for deep-seated inoperable tumors and infected tissues without needing surgical procedures for fiber removed.

Index Terms – biodegradation, bioactive glass, fiber, PDT

www.manaraa.com

1. INTRODUCTION

Photodynamic therapy (PDT) is an emerging therapeutic modality for cancers and infectious diseases based on the light-induced cell death [1-2]. Light-activated reactive oxygen species (ROS) destroys the tissue with three required ingredients which are light (mostly visible range), oxygen dependent photosensitizer (mostly porphyrin-based) and tissue oxygen. This approach is particularly promising because of the use of non-ionizing radiation (visible to near IR), minimally invasive in nature, highly portable and low cost procedure.

However several challenging technical issues exist for PDT to become one of mainstream cancer treatments including its limited application to surface treatment, highest possible single dose of light and photosensitizer per outpatient visit (as opposed to low dose repetitive interventional therapy) and low efficiency for large solid tumors with hypoxic environment owing to oxygen unavailability. Accordingly, an emerging approach has been identified as a new direction in PDT development which focuses on delivering the optimal light and photosensitizer separately over a period especially for brain tumors for which this therapeutic modality is more efficient appropriate [3-4].

This thesis focuses on an exemplary area that can benefit the most from biodegradable devices in the patient-specific, closed-loop PDT cancer therapy over an extended time frame (~months to year) because the aforementioned limitations can be overcome by proper light guiding device which are biodegradable. In this preliminary stage, a phosphate-based glass was used to prepare the core of light-guiding fiber, while the surrounding solution serving as cladding.

www.manaraa.com

2. FIBER OPERATION CONCEPT

A niche area that can be benefited the most from biodegradable devices is the patient-specific, fractionated, closed-loop PDT cancer therapy over an extended time frame (e.g., months to a year) because the aforementioned limitations can be largely overcome. This approach has been identified as a new direction in PDT development and termed as "metronomic PDT", focusing on how to deliver the optimal light and photosensitizers continuously over days or weeks, especially for brain tumors for which this therapeutic modality is more effective and appropriate [5].

Fig. 2.1. is a desired behavior of biodegradable optical devices utilized in the PDT for cancer. Light-guiding devices (e.g., optical fibers) can deliver a localized, optimal dose of light to deep locations (e.g., several inches). Although interstitial illumination with laparoscopes is conducted as an intraoperative adjuvant treatment, it is mostly limited to single therapy that requires repeated open surgeries if the cancer recurs. With implantable biodegradable devices with percutaneous couplers, long-term monitoring and therapeutic procedures will be possible during the intended device's lifetime (i.e., intended therapeutic period) without any concern for an additional surgical procedure to remove them.

Additionally, if biodegradable hollow devices are available, repeated localized delivery of required amounts of oxygen and optimal doses of photosensitizer are possible. This is expected to maximize the chance of success for hypoxic tumors and minimize the side effects related to patient's light sensitivity. Recent research on the photosensitizers

www.manaraa.com

has focused on improving their selectivity and efficiency in targeting only the malignant tissues [6].

Furthermore, the physiological parameters (e.g. oxygen, glucose, temperature, dose, etc.) within the tumor tissue are the core parameters of explicit dosimetry during PDT to evaluate the effectiveness of the therapy [5]. Therefore, a sensor-embedded light delivery probe will provide an additional merit to the proposed device.

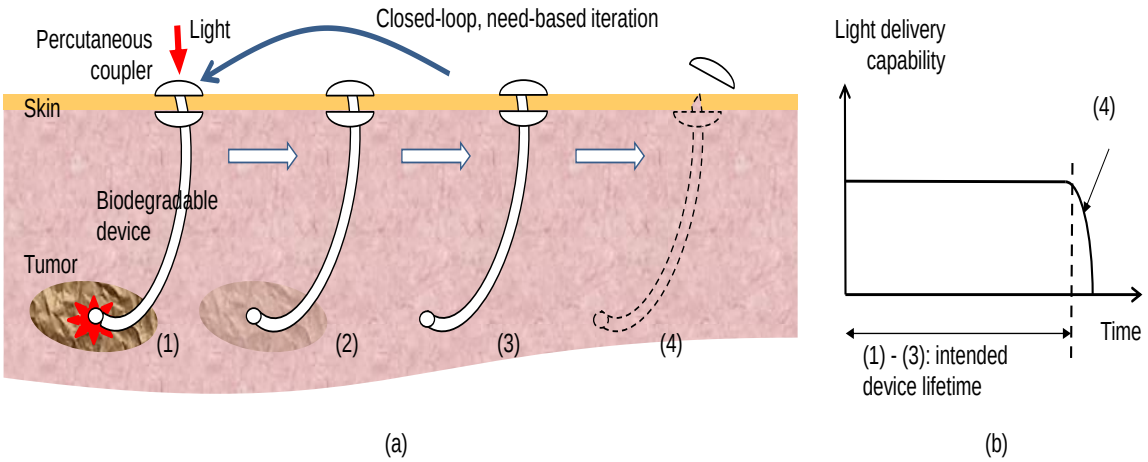

Figure 2.1. Biodegradable Fiber Operation Concept. Biodegradable device concept of implanted photodynamic therapy (PDT) for cancer. (a) Expected device biodegradation behavior without the need of removal surgical procedure. (b) "Sudden failure" of the device after the designed device lifetime (i.e., intended therapeutic period).

www.manaraa.com

3. EXPERIMENTAL DETAILS

3.1. FIBER PREPARATION

Bioactive phosphate based fiber is prepared by grinding sodium dihydrogen phosphate monohydrate ($NaH_2PO_4 \cdot H_2O$, ACS 98.0~102.0%) and calcium sulfate dibasic ($CaSO_4 \cdot 2H_2O$, ACS 98% extra pure) in a mortar for 10 min. The fine ground powder was mixed with phosphoric acid (H_3PO_4, ACS 85%) in a platinum crucible. The primary components were mixed at different weight percentage and ratio is given in Table 3.1. The crucible was then placed in an annealing furnace at 500˚ C for 16~18 hours. Afterward the platinum crucible is kept in a melting furnace at 1200˚ C for one hour while the melt is stirred every 15 minutes. Then the temperature of the furnace was reduced to 1100˚ C and soaked for one hour. After one hour the platinum crucible was removed and fibers were pulled after cooling for 2~3 minute at room temperature by hand. Approximately 200 µm diameter fiber was pulled from the soaked and cooled liquid glass.

Table 3.1. Fiber Composition.

Ingredient	Wt%
Na_2O	30
CaO	20
P_2O_5	50

www.manaraa.com

3.2. DISSOLUTION BEHAVIOR

Sample fiber of 200 µm diameter and approximately 70 mm length was kept inside a container of phosphate buffer solution of 300 mL to be completely submerged in phosphate buffer solution. Periodically the fiber was taken out from buffer solution and dried using hot dry air and weighed with a micro-balance (AE 240, Metler Toledo). Diameters at different location were measured with micrometer (Series 293-340, Mitutoyo). To observe the dissolution behavior of the fiber at different dissolution time, optical microscope (KH-8700, Hirox) was used to observe the cross-section.

3.3. OPTICAL PROPERTIES OF BULK GLASS

The melted glass is poured into a cylindrical mold of stainless steel and annealed at 350˚ C for 30 minute followed by room temperature cooling. Phosphate based glass rod measures 14 mm in diameter and 3 cm in length. Circular bioactive phosphate glass discs of approximately 3-4 mm thick were prepared by slicing cylindrical glass rod using a low speed saw (Isomet, Buehler). The glass discs were cleaned using acetone and then mounted on aluminum holders using a thermo plastic product (Brewerbond 220, Brewer Science).The top surface of the aluminum holder is covered with a thin coating of thermo plastic. It was heated on a hot plate at 80^{o} C for 10 minutes, 130^{o} C for 10 minutes and at 200^{o} C for 2 hours followed by cooling. Once it reached room temperature, it was again heated to 130^{o} C and the glass discs were placed on top and slightly pressed followed by cooling. The bonding between the glass disc and the aluminum holder was very strong at room temperature.

www.manaraa.com

The next step was polishing and grinding with automatic polisher (Tegramin30, Struers). Table 3.2. shows the process steps of grinding and polishing conducted in this study. First step was to bring the top surface of all the mounted glass wafers to a level for which grinding is done using a SiC foil of grit size of 76 µm for 30 seconds using 90 N force. Similarly the remaining polishing steps are carried out down to the grit size of 5 micron as mentioned in the table. DP-Yellow was used as lubricant during this procedure which is an ethanol based agent. The discs are then demounted by heating the aluminum holders to a temperature of 130^{o} C and sliding the wafers off the holders. The wafers are then cleaned ultrasonically in 1-dodecene twice for about 15 minutes, followed by one more ultrasonication step in isopropanol for 15 minutes. They are then sprayed with isopropanol and then blown dried using high purity nitrogen gas.

The final discs after the last step were approximately 1 mm thick with a highly reflective surface. The discs were then placed inside prism coupler (Metricon, Model 2010M) for refractive index measurement at 632 nm wavelength. Also the disc was placed in spectrophotometer (Genesis 10uv, Thermo Scientific) to measure transmission and absorption coefficient. Measurements were carried out from 190 nm to 1100 nm at 1 nm step size.

Table 3.2. Polishing Steps.

Step No	Grit Size (µm)	Polishing Agent	Force (N)	Time/Removal
1	76	SiC Foil	90	30 seconds
2	32.5 ~ 36	SiC Foil	90	300 µm
3	16.7 ~ 19.7	SiC Foil	90	200 µm
4	4.5 ~ 6.5	SiC Foil	90	>3 minute

www.manaraa.com

For refractive index measurement of phosphate buffer solution (PBS), ellipsometry technique [7-11] was used. Sample solution were placed in a known refractive index dish and 5 ml of solution was placed inside dish to create a thin film of solution and ellipsometer was scanned from 600 nm to 700 nm wavelength and real part of refractive index was measured.

3.4. TRANSMISSION PROPERTIES OF FIBER

Pulled fiber of 200 µm diameter was used for propagation loss measurement. Fiber of approximately 150 mm length was taken and both ends were cut sharply with optical slicer and one end was aligned to the output of the laser source (632 nm, 0.5 mW He-Ne polarized, Edmund Optics). This wavelength is used for one of the most common photosensitizer (e.g. protoporphyrin) [12]. The other end was placed inside the collection chamber of power meter (Model 2935C, Newport) to measure transmitted power was measured. Afterward, 25 mm fiber from the power meter end was repeatedly cut sharply and again transmitted power was measured. Subsequent power reading was calculated and propagation loss was measured in dB/km using the equation 1 stated below [13].

$$P_{loss} = \frac{-10\log(P_1 / P_2)}{L_1 - L_2} \tag{1}$$

where P_1 is the output power at length L_1 and P_2 is the output power at length L_2 respectively, while L_1 is longer than L_2.

Fibers of 200 µm diameter and 100 mm length were placed inside a black sample container (75x40x100 mm^3). The two ends of fiber were cut sharply. One end was aligned to laser source output, while the other being inside the collection chamber of

www.manaraa.com

optical power meter. Sample container was filled with 300 mL of phosphate buffer solution (PBS, pH 7.4, Sigma Aldrich) at room temperature and transmitted power was periodically measured until the fiber completely dissolves in approximately 10 days.

An optical simulation software (Mode Solution, Lumerical) was used for the simulation of transmission through fiber. The starting core diameter was 200 µm which decreases with respect to time as the fiber dissolves. The change of diameter was taken from experimental data obtained from dissolution experiment. The surrounding PBS was considered as cladding layer with constant refractive index. Two ports were placed at two ends of fiber and scattering parameter S21 was calculated which reflects the transmitted power. A conceptual diagram is shown in Fig. 3.1.

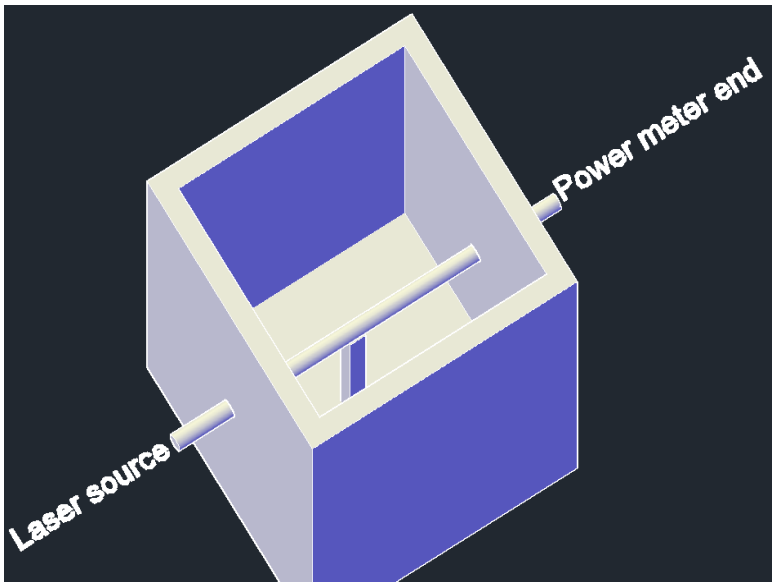

Figure 3.1. Conceptual Diagram Of Transmission During Dissolution.

www.manaraa.com

4. RESULTS AND DISCUSSIONS

4.1. REFRACTIVE INDEX

Refractive index of phosphate buffer solution measured using ellipsometry was found approximately 1.34. Fig. 4.1. shows the refractive index measured from 600 nm to 700 nm. At 632 nm the refractive index for phosphate buffer is found approximately 1.3369 with a standard deviation of 0.22%.

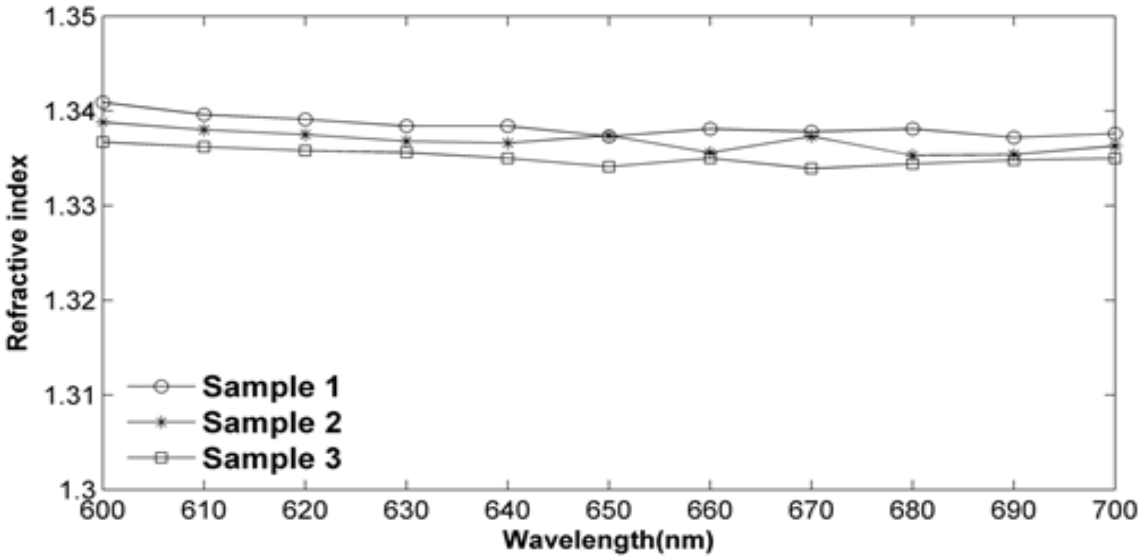

Figure 4.1. Refractive Index Of Phosphate Buffer Solution.

Refractive index of phosphate-based glass measured with prism coupler was 1.5225 (standard deviation = 0.02 %; n=3). This indicates the glass can be used as a light guiding fiber submerged in phosphate buffer solution as the refractive index is higher

www.manaraa.com

than that of the solution to support multiple propagation modes and a high numerical aperture 0.72 based on the equation 2.

$$NA = n\sin\theta = \sqrt{n_1^2 - n_2^2} \tag{2}$$

where NA is numerical aperture, n is the refractive index of the medium with light source, n_1 is the refractive index of core and n_2 is the refractive index of cladding

High numerical aperture essentially secures the insertion of a large portion of the light incident while multi-modes ensure the availability of higher transmitted power per wavelength.

4.2. TRANSMISSION/ABSORPTION OF BULK GLASS

Fig. 4.2. (a) and (b) shows the transmission and absorption spectra. The transmission and absorption are defined as follows shown in equation 3 and 4.

$$T = (I / I_o) * 100 \ [\%] \tag{3}$$

$$A = 2 - \log_{10}(\%T) \ [\text{unit-less}] \tag{4}$$

where I_o is blank reference intensity and I is sample intensity respectively

Transmission is initially low and rises sharply at the UV range reaching approximately 90 percent while at 400 nm. After that a minor fluctuation is observed in the transmission spectra while the average stays at approximately 90 percent. An opposite response is observed in the absorbance. At near ultraviolet region, absorbance is high and drops to very low value near 350 nm.

This result indicates that the proposed glass fiber of this composition can effectively deliver the expected wavelength (632 nm) to inside body during the therapeutic procedures.

www.manaraa.com

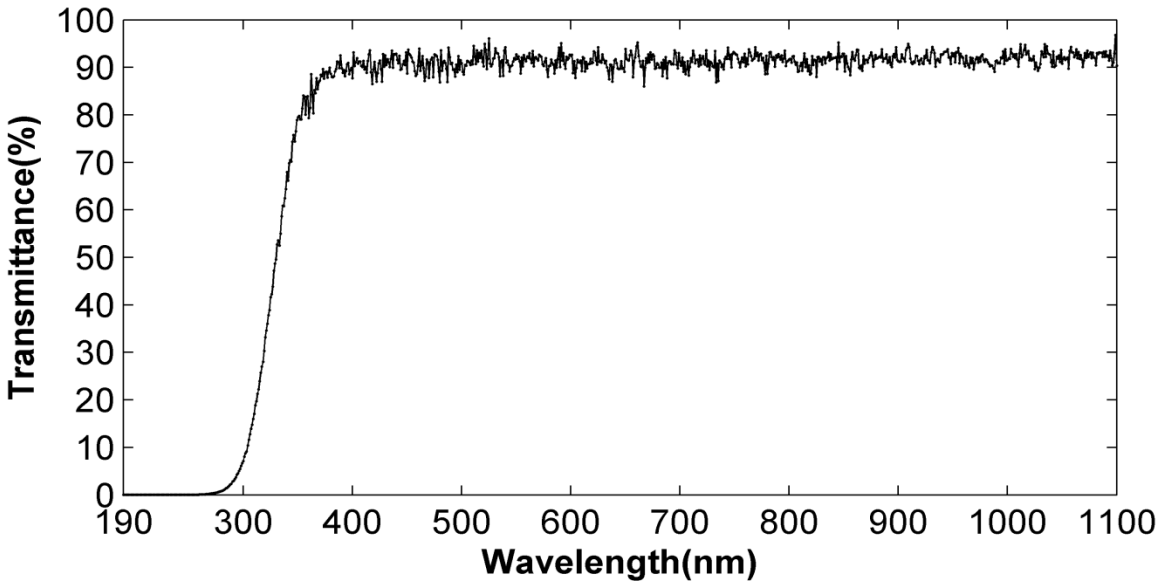

Figure 4.2. Transmission/Absorption. (a) Transmission spectra of bulk phosphate glass (Thickness=1mm).

4.3. PROPAGATION LOSS OF FIBER

Propagation losses measured are shown in Table 4.1. Overall it, turned out that the fiber has the propagation loss of approximately 14.5 dB/m at 632 nm wavelength. Although propagation loss varied but with low standard deviation and could be resulted from manmade inconsistency during cutting of fiber or incoherent dispersion from the receiving end due to unseen fiber cross-section. This loss is significantly high compared to those of conventional silica based fibers (usually less than 10 dB/km) used in telecommunication. However, since the required depth of implantation for therapy is only a couple of feet deep, this loss is not a critical problem for the proposed applications.

4.4. TRANSMISSION DURING DISSOLUTION

Dissolution behavior of phosphate glass fiber is shown in Fig. 4.3. Dissolution

www.manaraa.com

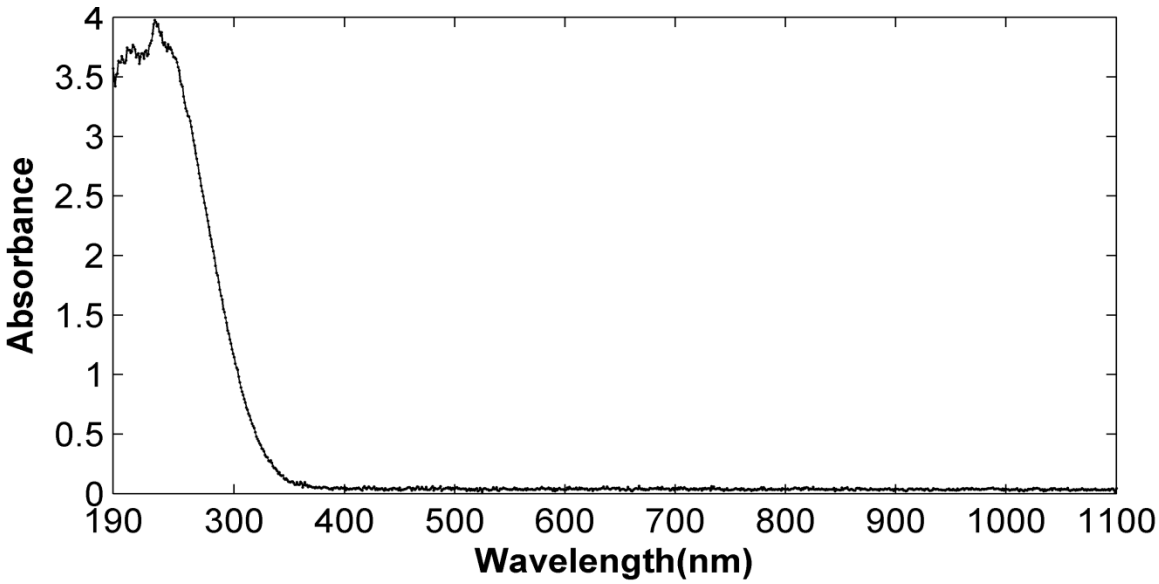

Figure 4.2. Transmission/Absorption. (b) Absorption spectra of bulk phosphate glass (Thickness=1 mm) (cont.).

Table 4.1. Propagation Loss.

Sample	Average (dB/m)	Standard Deviation (dB/m)	No of Measurements
1	14.19	0.32	5
2	14.79	0.21	4
3	14.13	0.28	4

rate depends on several factors such as mechanism of reacting layer formation, exposed surface area, composition of phosphate buffer solution and temperature. The dissolution rate was approximately 3.5 mg/hour with the original surface area approximately 0.43 cm^2. This rate is comparable with those of other phosphate-based glass material which are within the range of approximately 4 mg/hour [14].

Transmission through the phosphate-based fiber over the course of dissolution time is plotted in Fig. 4.4. The decrease in transmission is mainly due to the reduction of

www.manaraa.com

fiber (i.e. cross-sectional area) during dissolution. In addition, the reaction layer on the surface has different refractive index, while the phosphate buffer which acts as cladding also has varying refractive index over time due to ionic accumulation. Other factors also influence this change in transmission including porosity and surface roughness of reaction layer.

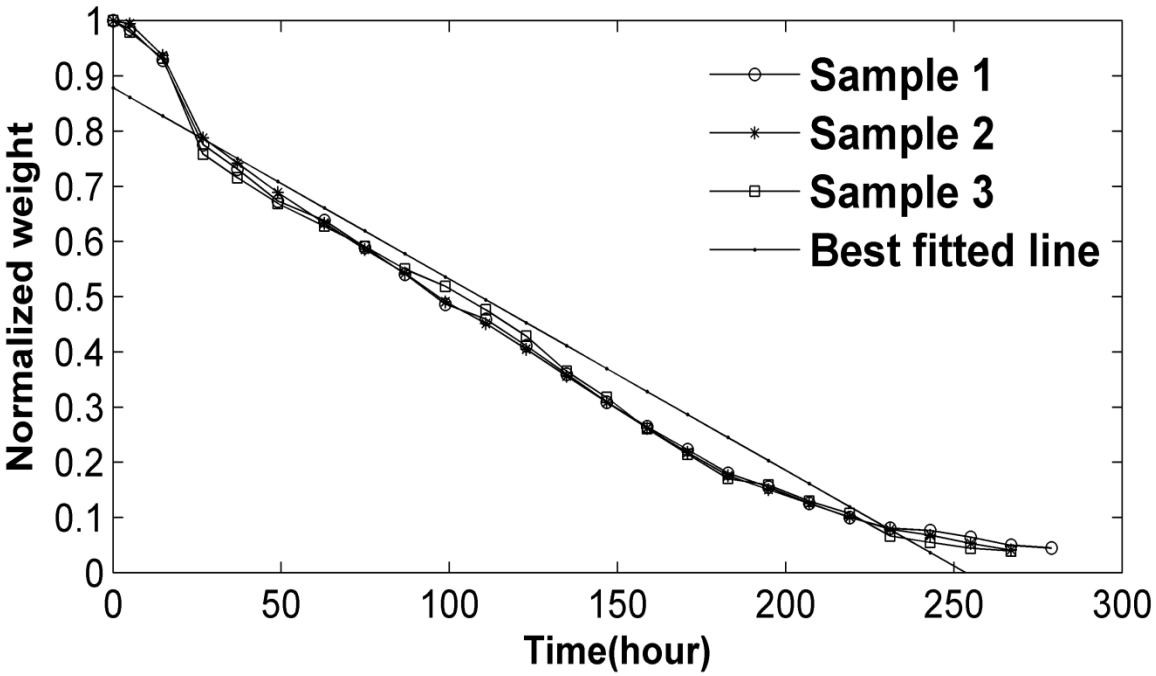

Figure 4.3. Dissolution Behavior Of Phosphate Fiber. Diameter: 200 μm, length: 70 mm, 21 ^{o}C.

4.5. SIMULATION

Simulation result of transmission during dissolution is shown in Fig. 4.4. The simulation was based on the separately measured diameter over time with different fiber samples. To utilize this data in simulation, diameters were converted to equivalent time

www.manaraa.com

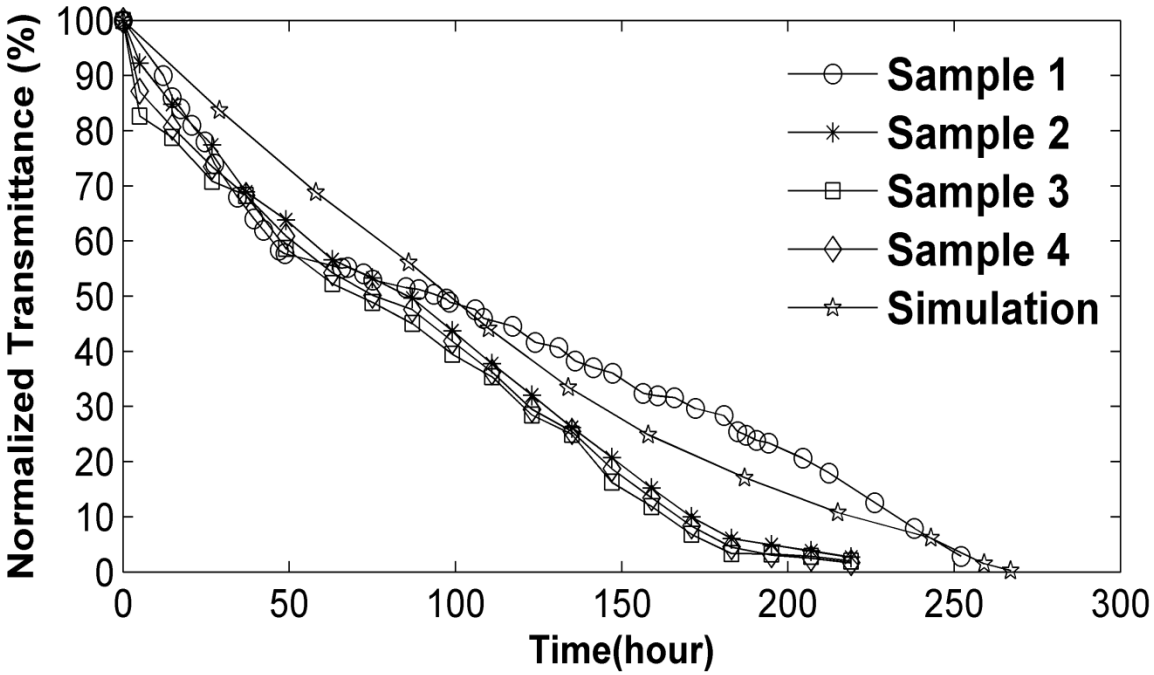

Figure 4.4. Transmission Change During Dissolution Of Fiber In PBS. Diameter: 20 µm, length: 100 mm, 21 ^{o}C.

period immersed in P.B.S. In simulation, the diameter was the only variable considered while the refractive indexes of fiber and phosphate buffer solution remain constant which is different in real situation. Also the simulation is done only within the portion of fiber submerged in phosphate buffer, while in experimental procedure there are two distal ends which are not immersed in PBS for laser sourcing and detection. Potential high scattering loss at this area where unchanged fiber and dissolved fiber meets was not reflected in the simulation. Also due to the limitation of modeling software, the surface roughness of reaction layer was not considered. Overall, the experimental and simulation results agree well despite the simplicity of simulation model and various deviations from the real experiment.

www.manaraa.com

5. CONCLUSION

Feasibility of a biodegradable light-guiding optical fiber built with reactive phosphate-based glass was demonstrated at a fixed wavelength (e.g. 632 nm) that is commonly used in photodynamic therapy. The experimental results of the change in transmission during dissolution are in good agreement with a simulation model. Therefore the use of biodegradable fiber made of reactive glass is expected to be a viable approach to develop reliable light-guiding device for therapeutic applications during an intended operational life time followed by steep degradation by structural disintegration. Future work includes the demonstration of a complete device structure with core and cladding with two different glass compositions.

www.manaraa.com

REFERENCES

[1] S. K. Bisland, L. Lilge, A. Lin, R. Rusnov, and B. C. Wilson, "Metronomic photodynamic therapy as a new paradigm for photodynamic therapy: rationale and preclinical evaluation of technical feasibility for treating malignant brain tumors," Photochem Photobiol, vol. 80, pp. 22-30, Jul-Aug 2004.

[2] D. E. J. G. J. Dolmans, D. Fukumura, and R. K. Jain, "Photodynamic therapy for cancer," Nat Rev Cancer, vol. 3, pp. 380-387, 05//print 2003.

[3] T. J. Dougherty, C. J. Gomer, B. W. Henderson, G. Jori, D. Kessel, M. Korbelik, et al., "Photodynamic therapy," J Natl Cancer Inst, vol. 90, pp. 889-905, Jun 17 1998.

[4] Z. Huang, H. Xu, A. D. Meyers, A. I. Musani, L. Wang, R. Tagg, et al., "Photodynamic therapy for treatment of solid tumors--potential and technical challenges," Technol Cancer Res Treat, vol. 7, pp. 309-20, Aug 2008.

[5] A. Master, M. Livingston, and A. Sen Gupta, "Photodynamic nanomedicine in the treatment of solid tumors: perspectives and challenges," J Control Release, vol. 168, pp. 88-102, May 28 2013.

[6] B. C. Wilson, S. K. Bisland, A. Bogaards, A. Lin, E. H. Moriyama, K. Zhang, et al., "Metronomic photodynamic therapy (mPDT): concepts and technical feasibility in brain tumor," in Biomedical Optics 2003, 2003, pp. 23-31.

[7] R. Azzam, "A and Bashara N M 1977 Ellipsometry and Polarized Light," ed: Amsterdam: North-Holland.

[8] L. Ward, "The accuracy of some mixed photometric and polarimetric functions in the determination of the optical constants of thin films," Journal of Physics D: Applied Physics, vol. 17, p. 1781, 1984.

[9] K. Vedam, "Spectroscopic ellipsometry: a historical overview," Thin solid films, vol. 313, pp. 1-9, 1998.

[10] D. Aspnes, "Expanding horizons: new developments in ellipsometry and polarimetry," Thin solid films, vol. 455, pp. 3-13, 2004.

[11] B. Ayupov, V. Gritsenko, H. Wong, and C. Kim, "Accurate ellipsometric measurement of refractive index and thickness of ultrathin oxide film," Journal of The Electrochemical Society, vol. 153, pp. F277-F282, 2006.

www.manaraa.com

[12] M. T. Wan and J. Y. Lin, "Current evidence and applications of photodynamic therapy in dermatology," 2014.

[13] I. Kaminow and L. Stulz, "Loss in cleaved Ti-diffused LiNbO3 waveguides," Applied Physics Letters, vol. 33, pp. 62-64, 1978.

[14] I. Ahmed, M. Lewis, I. Olsen, and J. Knowles, "Phosphate glasses for tissue engineering: Part 1. Processing and characterisation of a ternary-based P 2 O 5–CaO–Na 2 O glass system," Biomaterials, vol. 25, pp. 491-499, 2004.

www.manaraa.com

SECTION

2. CONCLUSION

Two test device structures to explore the concept of glass-based biodegradable devices, both for electrical and optical were designed and characterized. Specially formulated borate-based and phosphate-based glasses were used as the core materials for these applications. The electrical device demonstrated is a planar spiral inductor to investigate the passive element behavior on biodegradable substrate during dissolution of whole device structure in the simulated body fluids. Feasibility of a biodegradable light-guiding optical fiber built with phosphate-based glass was demonstrated at a fixed wavelength (e.g. 632 nm) that is commonly used in photodynamic therapy. Based on the results, it is highly feasible to implement a new class of devices that are fully functional only for a limited operational lifetime after implantation followed by rapid disintegration.

Desirable applications of implantable electrical biodegradable devices include biomedical sensors including pressure/flow monitoring for blood circulation problems, gastrointestinal tract disorders, head injuries, urinary problems and ocular diseases, to name but a few. Particularly biomechanical monitoring, such as stress/strain along bone fractures or associated with spinal fusion surgery, is highly desirable for orthopedic repair and rehabilitation.

The vision from the proposed optical device concept will have a large impact on future light based clinical paradigm especially for inoperable tumors. This concept is not limited to cancer therapy but applicable to deep-seated non-cancerous infective disease and graft-vs-host disease etc. Furthermore an emerging light based medical research area

www.manaraa.com

including optogenetic is another potential realm that can benefit from biodegradable optical devices. Therefore, outcome of this study is expected to continue lead to implementing this new class of implantable devices.

www.manaraa.com

APPENDIX A.

PROCEDURE FOR PREPARING BORATE GLASS WAFER

www.manaraa.com

Bioactive borate glass wafer is prepared by first making glass rods and by then slicing it into wafers using a low speed saw (Isomet, Buehler). Preparation procedure for glass rods and wafers is described in Table A.1. Glass composition is given in Table A.2.

The glass wafers were then mounted on an aluminum holder using a thermo plastic product, Brewerbond 220 (Brewer Science, Rolla, MO), so that they can be clamped into a specimen holder and then polished using an automatic polisher (Tegramin30, Struers). Mounting procedure is described in Table A.3. Table A.4. and A.5. covers the detailed procedure polishing and grinding.

After the polishing the wafers were then demounted and cleaned. Table A.6. records the procedure for demounting and cleaning glass wafers.

www.manaraa.com

Table A.1. Preparation Procedure for borate glass rods and wafers.

Sr. No.	Procedure
1	- Melting sodium tetraborate ($Na_2B_4O_7$) in a platinum crucible for 30 minutes at 1000˚C - Stirred every fifteen minutes using a pure silica rod
2	- Poured into stainless steel cylindrical molds preheated to 200˚C - annealed at 450˚C for 30 minutes - Cooled slowly (furnace normal cooling rate) to room temperature
3	- Cylindrical glass rod of approximately 1.4 cm diameter and 3cm length was formed - Glass rod formed is then wrapped using an insulation tape and mounted on the saw - A small weight is applied on the saw arm and the instrument was setup at 6 rpm - Glass wafers formed were 3~4 mm and afterward cleaned using acetone

Table A.2. Material composition for borate glass rods and wafers.

Component	Wt %	Mol %
B_2O_3	69.2	66.7
Na_2O	30.8	33.3

www.manaraa.com

Table A.3. Mounting procedure for wafers.

Sr. No.	Procedure
1	- Aluminum holder cleaned with acetone - Top surface of holder coated with a thin layer of Brewer Bond 220
2	- Holder heated on a hot plate - At 80^{o} C for 5 minutes - At 130^{o} C for 5 minutes - At 180^{o} C for 5 minute - Cooled to room temperature
3	- Holder again heated to 130^{o} C - Glass wafer was placed on top and slightly pressed - Cooled to room temperature - Very strong bonding between the glass wafer and the aluminum holder

www.manaraa.com

Table A.4. Procedure for polishing and grinding glass wafer.

Sr. No.	Procedure
1	- Six aluminum holders mounted with glass wafers were clamped in a specimen holder - Insert the holder in the automatic polisher(Tegramin30, Struers)
2	- Mount MD-Gekko (300 mm magnetic pad for attaching SiC foils) on MD-Disc (drive plate) - An alcohol based lubricant (DP-Lubricant Yellow, Struers) is used just enough to keep the surface moist through all the polishing and grinding steps
3	- Drive plate is set at 300 RPM* - Head is set at 150 RPM - Co-rotation of both drive plate and head (drive plate 300 RPM, head 150 RPM)

* Drive plate is set at 150 RPM for diamond polishing stage

** Same rotation speed for drive plate and head might result in better polishing as it may damage the surface of the wafer less

www.manaraa.com

Table A.5. Sequential polishing and grinding with different grit size.

Step No	Grit Size (um)	Polishing Agent	Force (N)	Time/Removal
1	76	SiC foil	90	30 seconds
2	32.5~36	SiC foil	90	100 um
3	16.7~19.7	SiC foil	90	50 um
4	4.5~6.5	SiC foil	90	1 minute
5	3	Diamond Suspension	60	3 minutes
6	1	Diamond Suspension	60	3 minutes
7	0.25	Diamond Suspension	60	3 minutes

Table A.6. Procedure for demounting and cleaning glass wafer.

Sr. No.	Procedure
1	- Aluminum holders heated to a temperature of 130° C - Wafers were slid off the holders
2	- Wafers were cleaned ultrasonically in 1-Dodecene twice for 15 Minutes each - Ultrasonication was done in isopropanol for 15 minutes - Wafers were wiped clean using 100% continuous polyester wipes (TX 1009 Alpha Wipe) - Wafers were sprayed with isopropanol and then blown dried using high purity nitrogen gas.

www.manaraa.com

APPENDIX B.

PROCEDURE FOR THIN OXIDE FILM COATING AND INDUCTOR PATTERNING

www.manaraa.com

Borate glass wafers were coated with silicon oxide using DC sputtering. A shadow mask was used to pattern gold thin film inductor afterward on top of silicon oxide. Table B.1. describes the methods used for deposition of silicon oxide and gold. Fig. B.1. shows a conceptual silicon oxide coated wafer.

Figure B.1. Conceptual representation of coated wafers.

Table B.1. Methods used for deposition of silicon oxide and gold.

Method	Working parameters
Silicon oxide RF sputtering	- Deposition time: 3.5 hours (30 min's cleaning and 3 hours deposition) - Total working pressure: 8×10^{-3} torr (7.2×10^{-3} torr argon and 0.8×10^{-3} torr oxygen) - Ratio of argon to oxygen: 8:1
Shadow mask	- Stainless steel 4 mil thick mask (Stencil) - Inner diameter 1 mm, Outer diameter 6.6 mm, 8 turn, Line width 0.2 mm and Line spacing 0.15 mm
Gold deposition (Biorad E5400)	- Gas: Argon - Working Pressure: 80 millitorr (Argon) - DC Current: 20 mA - Deposition time: 3 minutes

www.manaraa.com

APPENDIX C.

PROCEDURE FOR INDUCTOR PACKAGING

www.manaraa.com

To provide an equal exposed area to the solution in all the devices a nylon washer (inner diameter 11 mm) was glued to the wafer bottom surface of the device using silicone paste. This silicone formed a reliable water resistant bond with the wafer after curing. For connectivity up to vector network snalyzer (VNA), another 12 inch long 50 ohm characteristic impedence SMA to SMA connector was attached where one end was connected to SMA connector while the other end was attached to VNA machine. The SMA to SMA connector is already encapsulated with protective layer so silicone paste was applied at the joint to prevent water leakage or prevent contacting with water. Everywhere except the region defined inside the washer is coated with silicone paste including the junction between the extension SMA cable and the wafer. The device was then left for four hours for the silicone to cure. If any holes or uncoated areas were observed after curing then an additional layer of silicone was applied and then cured. Table C.1 shows the various steps involved in the building device. For all the in-vivo operations in future slow dissolving glass will be used for encapsulation instead of silicone and there will be no nylon washer involved.

www.manaraa.com

Table C.1. Procedure for packaging of device.

Sr. No.	Procedure
1	- Nylon washer (inner diameter 11 mm) was glued using RTV silicone (Dow Corning 3140) to the bottom surface of the device where no inductor lead is present
2	- SMA RF jack (Molex- A305789) was attached on the two ends of Inductor using silver paste (SPI- Z04969) - Curing was done at 50^{o} C at hot plate for 30 minute - After jack is attached securely then additional silicone is applied to cover the exposed area along with the jack followed by heat curing as mentioned above
3	- Another extension cable of 12 inch long SMA (M) to SMA (F) was connected to SMA jack after silicone encapsulation cured
4	- Joint between SMA cable and SMA jack was then covered with additional silicone to ensure no SBF solution can breach into device
5	- If any holes or uncoated areas were observed after curing then an additional layer of silicone was applied and then cured

www.manaraa.com

APPENDIX D.

SIMULATED BODY FLUID (SBF) RECIPE

www.manaraa.com

SBF was prepared according T. Kokubo et el. [1]. PH of SBF solution was 7.4. The protocol for preparing 1L SBF solution is charted below in Table D.1.

Table D.1. Protocol for SBF making.

Order	Reagent	Amount
1	NaCl	7.996 g
2	$NaHCO_3$	0.350 g
3	KCl	0.224 g
4	$K_2HPO_3.3H_2O$	0.228 g
5	$MgCl_2.6H_2O$	0.305 g
6	1M HCl	40 mL
7	$CaCl_2$	0.278 g
8	Na_2SO_4	0.071 g
9	$(CH_2OH)_3CNH_2$	6.057 g

www.manaraa.com

APPENDIX E.

PROCEDURE FOR CHARACTERIZATION OF BORATE GLASS

www.manaraa.com

Table E.1. shows the procedure and specification followed for borate glass characterization.

Table E.1. Material Characterization.

Method	Working parameters
Differential Thermal Analysis (DTA)	- Differential Thermal Analysis was performed using DTA7, Perkin Elmer. - Temperature was ramped at 10^{o}C per minute from 30^{o}C to 800^{o}C
Coefficient of Thermal Expansion (CTE)	- CTE was measured using L76, Linseis dilatometer - Temperature was ramped at 1^{o}C per minute from 71^{o}C to 550^{o}C
Surface Roughness	- 3D profiling image was also captured for both polish and unpolished surface using optical microscope KH-8700, Hirox
Hardness	- Micro-hardness tester Duramin A300, Struers was used to measure vickers hardness number and then converted to GPa(Giga Pascal) - Glass discs were polished at both side using the method mentioned above
Dissolution rate measurement	- Initial weight of bare glass disc was measured using analytical balance AE240, Metler Toledo - Each disc was immersed in 1L of SBF solution - The SBF solution container with glass disc was kept in an incubator Heratherm IGS 100, Fisher Scientific at 37^{o}C while solution was stirred at 10 RPM - Additionally dissolution data was taken for 22^{o} C and 50^{o} C to see the dependency of temperature on the dissolution rate.

www.manaraa.com

Table E.1. Material Characterization (cont).

Dielectric constant of borate glass	- Bioglass was prepared in rectangular form of 5”X3” with a thickness of 20 mm - Top and bottom surface were polished with SiC foil of 76µm grit size to make surface even to ensure no airgap between glass slab and waveguide - Open ended Coaxial method was used for measuring dielectric constant at R band (1.7~2.6 GHz) and S band (2.6~3.95 GHz)
Dielectric constant of SBF solution	- 1L of SBF solution was placed in a container - Open ended Coaxial method was used for measuring dielectric constant at R band (1.7~2.6 GHz) and S band (2.6~3.95 GHz) - Same rectangular waveguide was positioned using a micro-meter touching the liquid surface - Subsequent measurements were taken at different position e.g. surface level, below surface and above surface - Distilled water dielectric constant was measured at each band to validate the result as well

www.manaraa.com

APPENDIX F.

RESULTS OF BORATE GLASS CHARACTERIZATION

www.manaraa.com

Fig. F.1. shows the result for DTA measurement. This result gives glass transition temperature at 470^{o} C, glass crystallization temperature at 597^{o} C and glass melting temperature at 734^{o} C respectively. It is conclusive from the evidence that any additional device preparation process on the wafers should be done below the glass transition temperature which will not affect the hardness of wafer as mechanical stability is.

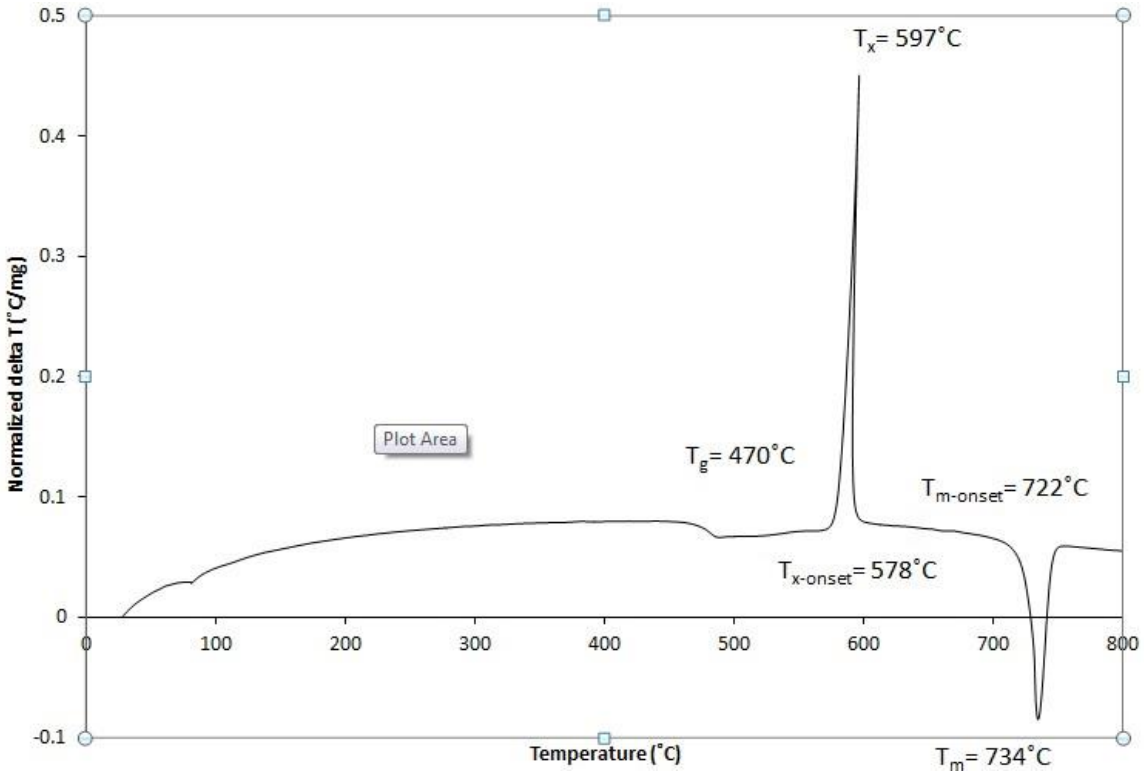

Figure F.1. Differential Thermal Analysis Result.

Fig. F.2. shows the thermal expansion coefficient result. As the result indicates the thermal expansion is very small at low temperature and gradually increases up to 450 ^{o} C and then start decrease. This phenomenon is due to the fact that the glass starts

www.manaraa.com

transitioning after that temperature as seen from DTA result. Also this is close to crystallization temperature where heat is actually released from the sample for structural change which explains the decrease in CTE value. Additionally CTE value for aforementioned temperature range is given in Table F.1.

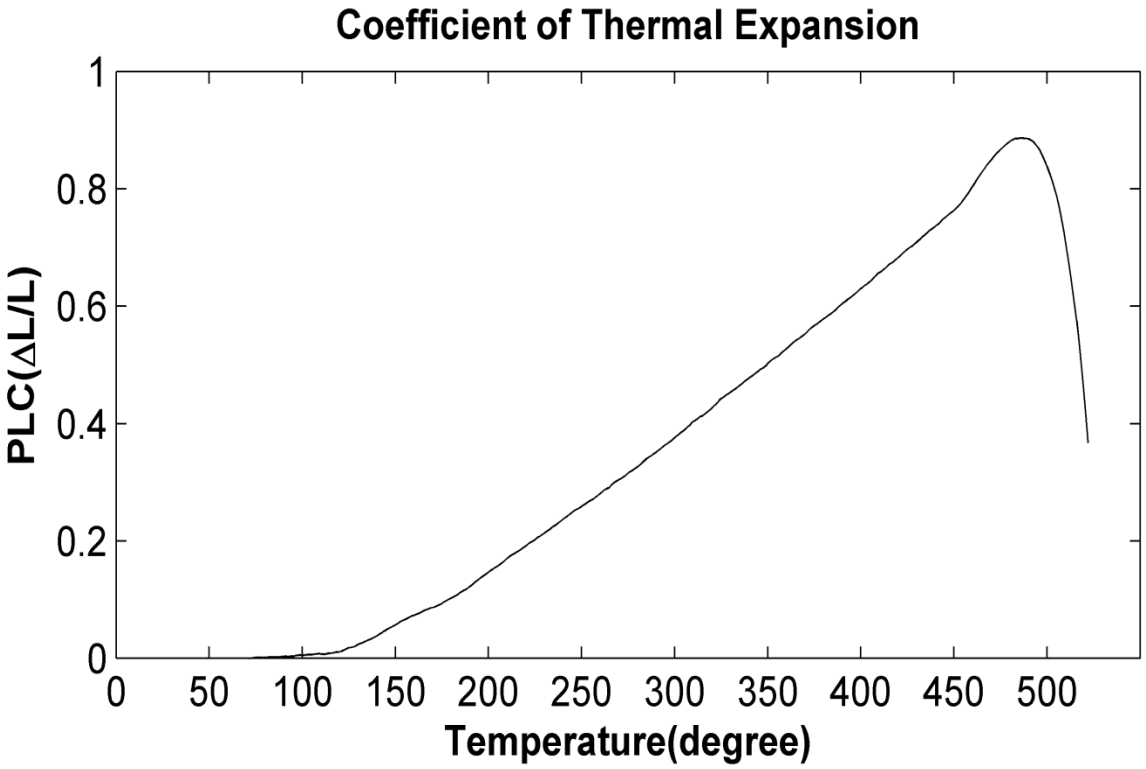

Figure F.2. Differential Thermal Analysis Result.

Micro hardness results are shown in Fig. F.4 for different samples. The result indicates higher hardness at lower load value which is expected. Hardness drastically reduces with higher load and be saturated starting at 0.5 N until it reaches 1.96 N after which the load creates fracture in the sample. It is clear from the result that after 1.96 N

www.manaraa.com

Table F.1. Coefficient of Thermal Expansion.

Temperature range (^{o}C)	Coefficient of Thermal Expansion (C^{-1})
71 ~ 100	1.63E-06
100 ~ 150	1.04E-06
150 ~ 200	1.79E-05
200 ~ 250	2.24E-05
250 ~ 300	2.35E-05
300 ~ 350	2.53E-05
350 ~ 400	2.56E-05
400 ~ 450	2.66E-05
450 ~ 500	1.50E-05

load, this composition loss rigidity and fracture occurs.

Fig. F.3. (a) and (b) represents the surface roughness before and after polishing captured by optical microscope.

Fig. F.5. shows the dissolution behavior at different temperature. As seen from the plot, increasing temperature increases the dissolution rate. Increment of dissolution rate is not linear with temperature.

Table F.2. shows the dielectric constant measured for three samples of borate glass at R band and S band. The average dielectric constant at R band is 8.4484-0.9033i and at S band 8.7688-0.3370.

Table F.3. shows the dielectric constant measured at R band and S band for the SBF solution. The average dielectric constant at R band is 68.0315-28.5438i and at S band 69.72274-26.1127.

www.manaraa.com

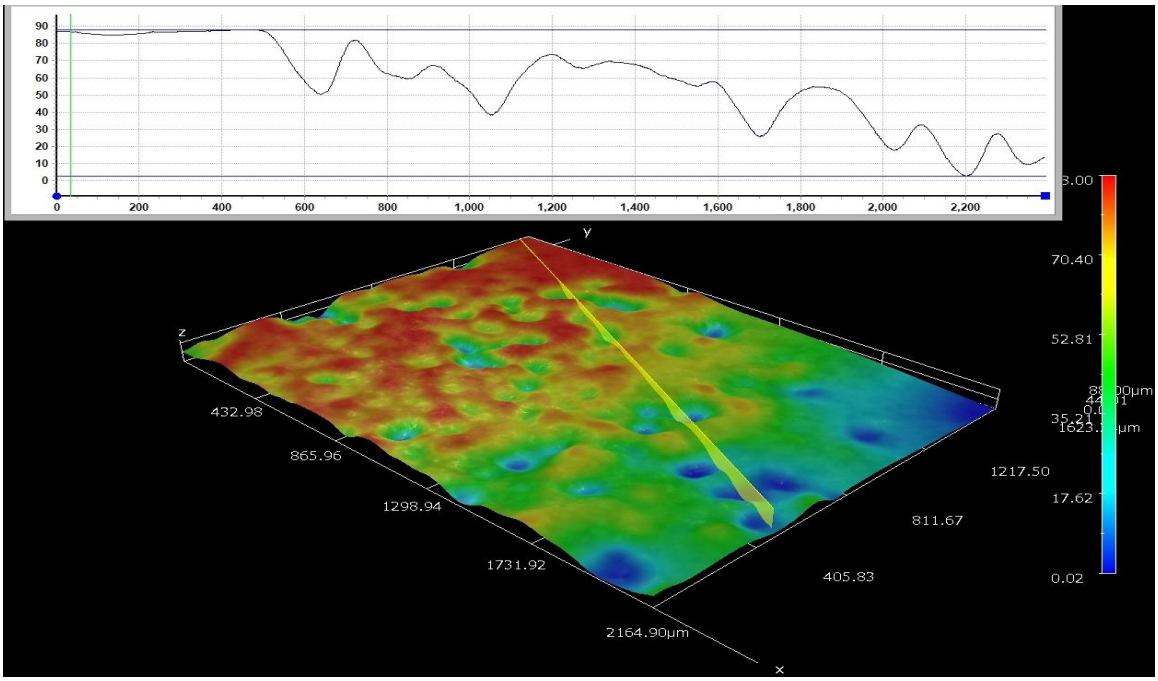

(a)

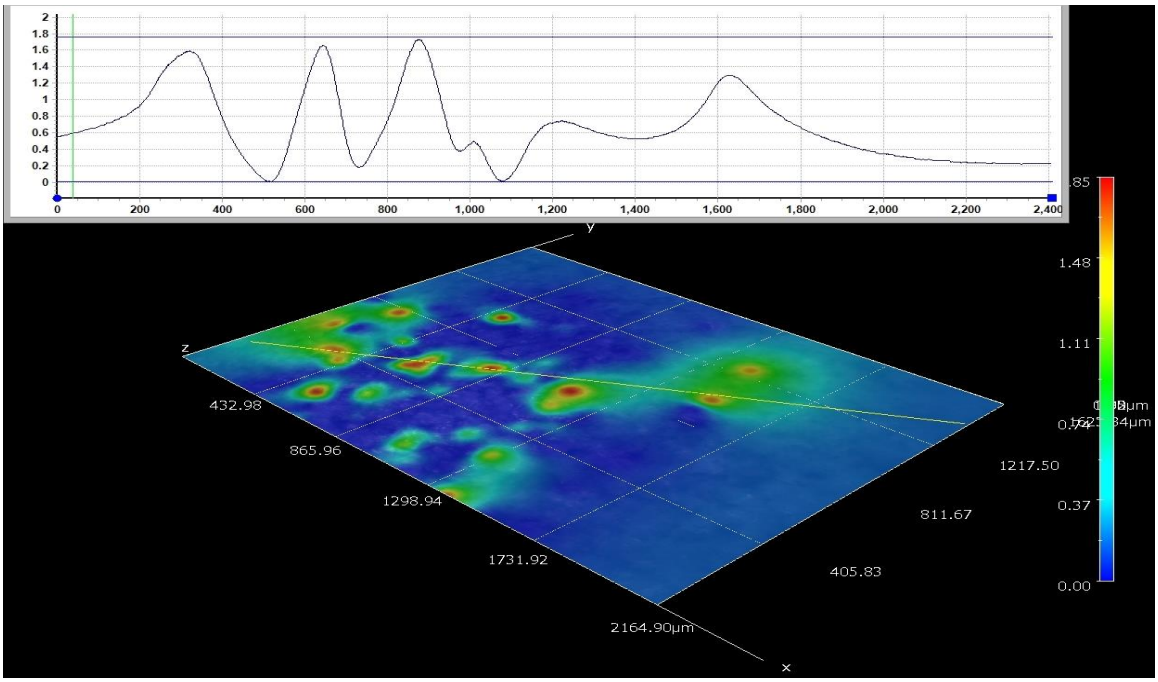

(b)

Figure F.3. Optical 3D profile images of the surface of (a) Unpolished surface and (b) Polished surface.

www.manaraa.com

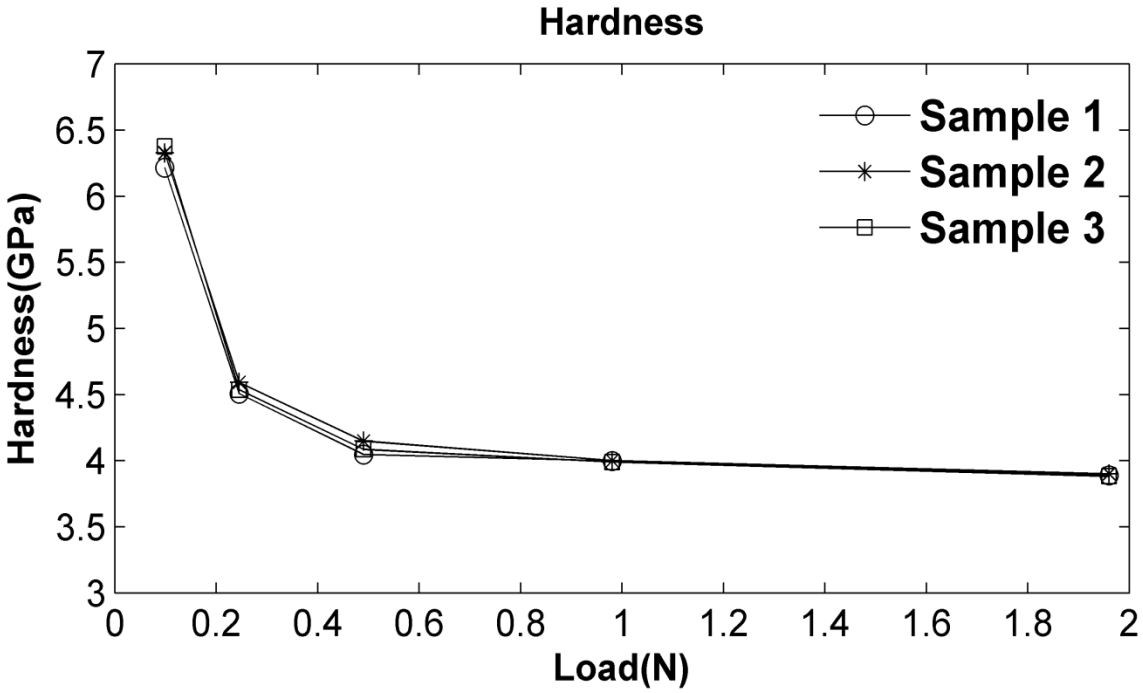

Figure F.4. Micro-hardness for borate based bulk glass.

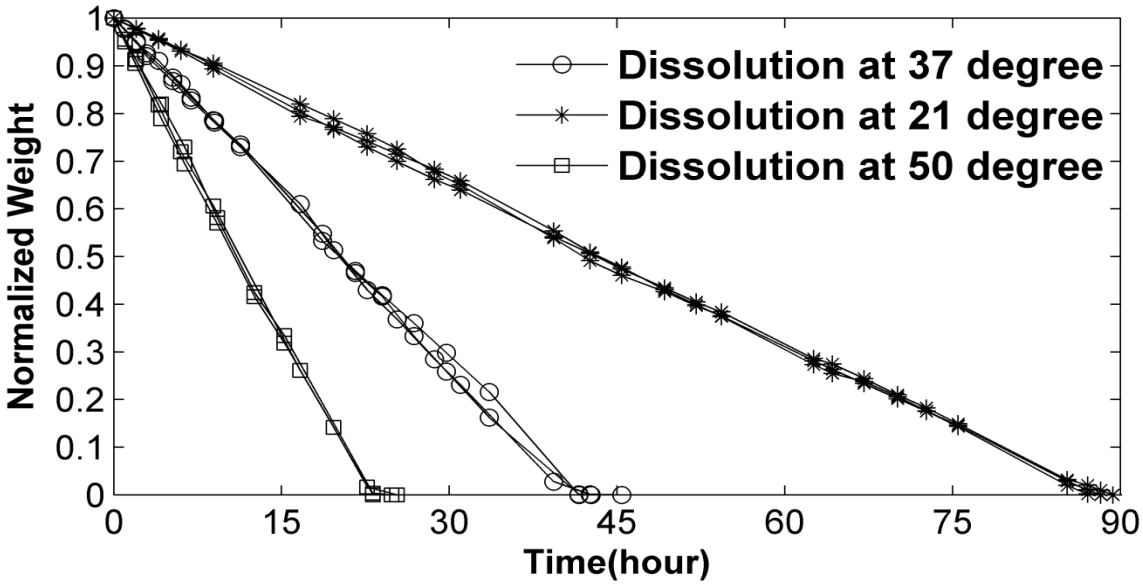

Figure F.5. Dissolution behavior of borate based glass wafer at different temperature.

www.manaraa.com

Table F.2. Complex dielectric constant of sodium borate glass.

Band	#1 average	#2 average	#3 average	Average	Standard deviation
R	8.5168 - 0.9116i	8.4299 - 0.8951i	8.3985 - 0.9031i	8.4484 – 0.9033i	0.06
S	8.8015 - 0.2609i	8.5764 - 0.3502i	8.9287 - 0.3998i	8.7688- 0.3370i	0.18

Table F.3. Complex dielectric constant of SBF.

Band	#1 average	#2 average	#3 average	Average	Standard deviation
R	69.0707 - 25.8473i	68.3089 - 30.3559i	66.7151 - 30.4283i	68.0315 – 28.5438i	0.39
S	69.6972 - 26.1025i	69.2398 - 29.0609i	68.8952 - 23.1748i	69.7227- 26.1127i	0.42

www.manaraa.com

APPENDIX G.

PROCEDURE FOR INDUCTOR CHARACTERIZATION

www.manaraa.com

1. Inductance calculation. Inductance value was calculated using the expression stated as Current Sheet Expression formula [3]. The expression is given below in equation G1.

$$L = \frac{\mu n^2 d_{avg} c_1}{2} (\ln(c_2 / \rho) + c_3 \rho + c_4 \rho^2) \quad \text{(G1)}$$

d_{avg} = average of inner diameter d_{in} and outer diameter d_{out}

n = number of turns

μ = Magnetic permeability

ρ = fill ration = (d_{out} - d_{in})/(d_{out} + d_{in})

c_1, c_2, c_3 and c_4 are constant given in Table G.1

Table G.1. Coefficient for Current Sheet Expressions.

Layout	C_1	C_2	C_3	C_4
Square	1.27	2.07	0.18	0.13
Hexagonal	1.09	2.23	0.00	0.17
Octagonal	1.07	2.29	0.00	0.19
Circle	1.00	2.46	0.00	0.20

2. Parasitic capacitance calculation. Parasitic capacitance was calculated using two methods. Theoretical calculation was done using the prescribed formula by Yue et el. [1]. Again the input impedence of the Device Under Test (DUT) was calculated from 1.5

www.manaraa.com

GHz to 3 GHz and from the two distinctive frequency input impedence, simple equation shown in equation G2 was solved to get the parasitic capacitances. For simplicity of theoretical modeling, a derivation of Yue's work was chosen for this work. The simplified design is shown below in Fig. G.1.

$$Z = \frac{R + jwL}{(1 - w^2 LC_v - w^2 LC_f) + jwR(C_v + C_f)} \tag{G2}$$

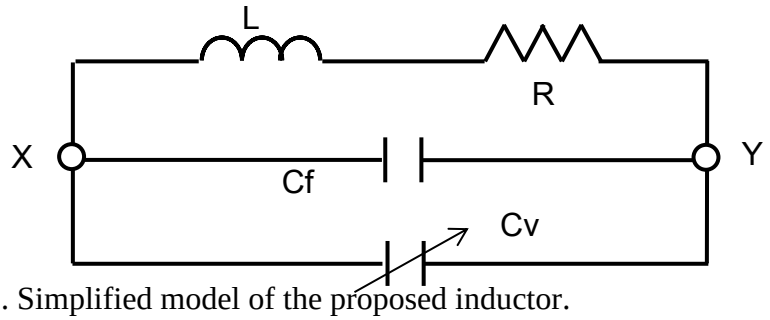

Figure G.1. Simplified model of the proposed inductor.

Here C_f is the fixed capacitance between spiral inductor coils filled by encapsulation layer, C_v is the summation of two capacitances which are C_{ox} and C_{sub} which are interwinding capacitances through silicon oxide layer and buried glass substrate layer.

3. S11 measurement and measurement error compensation. DUT was connected to a SMA RF connector and then an extension cable of SMA to SMA was connected to increase the portability and connectivity to VNA. It also allowed the DUT to be submerged in the 1 L solution of SBF. The addition of SMA jack and extension cable can influence the result highly in high frequency regime. So 1 port 3 Term error model formulated by Rehnmark [2] was used to obtain the error values which were subsequently

www.manaraa.com

deducted from measured response to get an actual response. The system model and the error terms are shown in Fig. G.2.

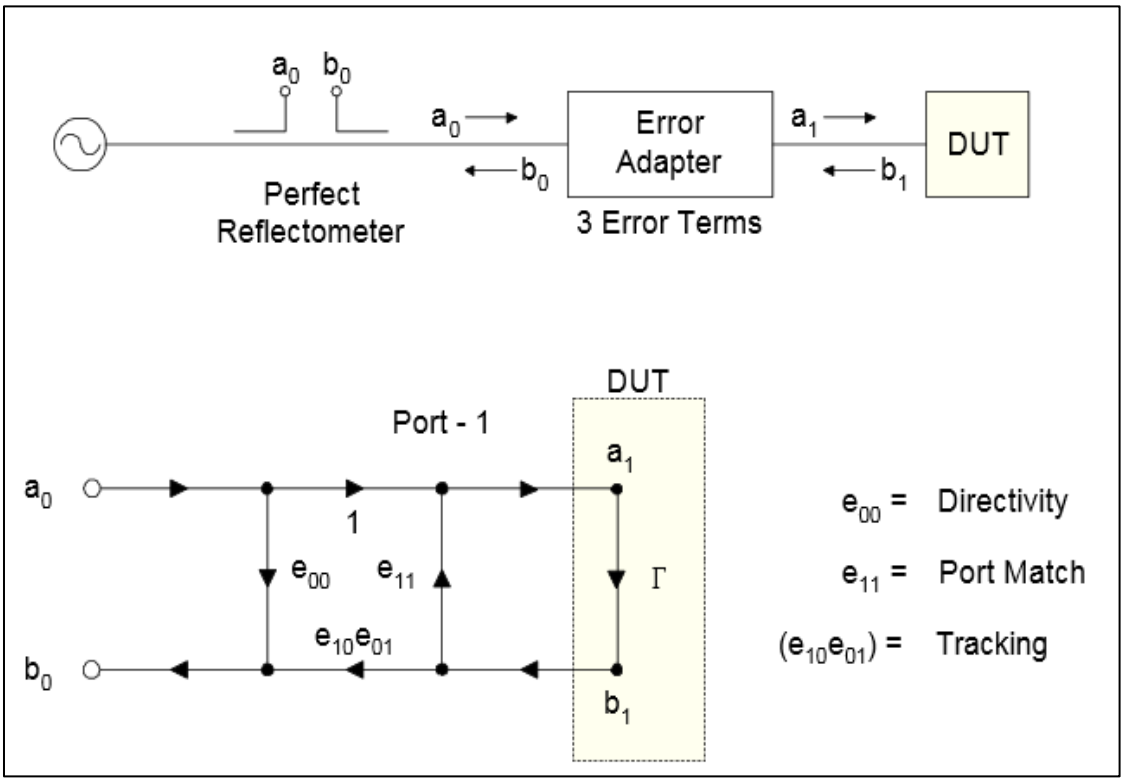

Figure G.2. System model and error terms.

Three known standard of short (0 ohm), open (∞ ohm) and load (50 ohm) were used and the measured value were stored. From measured result and known standard value the following equations were solved to get the error terms which represents the error values originated from extension cable and SMA jack. These error values were then subtracted from the actual DUT measured response to get the actual response of the DUT. Fig. G.3 shows the error model equation used in this paper.

www.manaraa.com

Measured	Actual
$\Gamma_{mi} = \frac{b_0}{a_0} = \frac{e_{00} - \Delta_e \Gamma_i}{1 - e_{11}\Gamma_i}$	$\Gamma_i = \frac{\Gamma_{mi} - e_{00}}{\Gamma_{mi} e_{11} - \Delta_e}$

$$\Delta_e = e_{00}e_{11} - (e_{10}e_{01})$$

For ratio measurements there are 3 error terms so equation can be written in linear form

$$e_{00} + \Gamma_i \Gamma_{mi} e_{11} - \Gamma_i \Delta_e = \Gamma_{mi}$$

With 3 different known Γ_i, measurement was taken and resultant 3 Γ_{mi} was found.

Then the following equations were solved for e_{00} , e_{11} and Δ_e

$$e_{00} + \Gamma_i \Gamma_{mi} e_{11} - \Gamma_i \Delta_e = \Gamma_{mi}$$

$i =$ 1, 2 and 3 and known standards were Open (∞ Ω), Short (0 Ω) and Load (50 Ω)

Figure G.3. Error model equations.

DUT, SMA jack and extension cable were encapsulated using silicone fixative leaving only the controlled exposed area on the bottom side of bioglass substrate. VNA machine was properly calibrated each time during the start of the experiment according to standard procedure. VNA provided S11 or reflection coefficient of DUT which is a direct expression for input impedence and given by

$S_{11} = \frac{Z_{in} - Z_o}{Z_{in} + Z_o}$ where Z_{in} = Input impedence of DUT and Z_o = Characteristic

www.manaraa.com

Impedence of VNA which is 50 ohm. Agilent E8753 was used during this measurement. During the S11 measurement the DUT was submerged in 1L solution of SBF and kept in an incubator (HeraTherm B37) at 37^{o} C.

4. Impedance and resistance monitoring. For the impedance monitoring of devices, one device was immersed in a jar filled with 1L of SBF constantly stirring at 10 rpm kept inside the incubator at 37 o C. Impedance monitoring was done using an electrochemical measurement system (PC4/750, Gamry). AC impedence measurements were taken at 1.0 kHz. DC resistance was taken using the same machine but using Chronoamperometry module where the voltage level of 0.1V and current were measured and the ration between voltage and current gives the DC resistance. Readings were taken till the device dissolved.

5. S11 simulation. Computer Simulation Technology (CST) software, microwave studio module was used for simulation. Actual device geometry was drawn according to dimension. Dielectric property for silicon oxide and silicone are taken from literature [3-4] which were used as the input parameter. As for dielectric strength of SBF and bioglass are not known so practical value measured before were used as input parameter. Simulation was performed in the sample frequency range at same interval like experimental measurement of S11 parameter.

www.manaraa.com

APPENDIX H.

PROCEDURE FOR PHOSPHATE GLASS CHARACTERIZATION

www.manaraa.com

1. Differential Thermal Analysis. Differential thermal analysis (DTA) of bioactive phosphate glass was conducted with a differential thermal analyzer (DTA7, PerkinElmer). Fiber was grounded in a mortar and the finely grounded powder (< 74 µm particle size) placed in DTA sample holder. The temperature was ramped at 10^{o} C per minute and ranged up to 900^{o} C.

2. Coefficient of Thermal Expansion. Coefficient of Thermal Expansion (CTE) was measured on bulk sample of glass rod with 14 mm diameter and 26 mm length. The glass rods were polished with SiC foil of 76 µm at both ends for less than 1 minute to make even surface and parallel to each other. Later the sample was placed inside dilatometer (Model 1600, Orton). Data generated from the machine gave percentage of length change (PLC%) and temperature (T). Using equation H1, CTE was measured at different temperature range.

$$PLC = \frac{\Delta L}{L_0} = \alpha \Delta T \tag{H1}$$

where α is CTE and ΔT is temperature difference.

3. Hardness. Hardness of bulk sample and fiber were calculated using micro-hardness tester (DuraScan G5, Struers) [1-2]. Bulk sample and/or fiber were placed in a plastic holder of cup shape coated with vaseline and an epoxy resin was poured inside. After resin is cured at room temperature then the cylindrical shape epoxy with sample inside was taken out from plastic holder. This cylinder was polished using SiC foil (76 µm grit size) to get an even and shiny surface on top. Micro-hardness test load was varied from 9.81 mN to 4.91 N and corresponding Vicker number was observed. Equation H2 was used to convert vicker number to hardness in terms of giga pascal (GPa).

$$H = 0.009807 * HV \text{ [GPa]} \tag{H2}$$

www.manaraa.com

where *HV* is Vickers Hardness.

4. Elemental Analysis. The elemental composition of the surface of fiber samples was analyzed using scanning electron microscope (Nanolab 600, Helios) to identify the thickness of reacting layer formed over the fiber surface after placing in phosphate buffer solution. Also energy dispersive spectroscopy (EDS) equipped with the microscope was used to analyze the elemental composition of this reacting layer. Oxford INCA software was used for EDS. An accelerating voltage of 5 kV and a current of 0.17 nA was used. 20 seconds of live time was used for spectrum collection at a working distance of 5 mm.

www.manaraa.com

APPENDIX I.

RESULTS OF PHOSPHATE GLASS CHARACTERIZATION

www.manaraa.com

Fig. I.1 shows the DTA result where one glass transition temperatures (Tg_1), one crystallization peaks (Tp1) with four different inflection point and one melting temperature (Tm) is observed. Tg_1 is found at 394^o C. Peak for crystallization found at 538^o C and four inflection points were found at 469^o C, 490^o C, 513^o C and 532^o C. Tm is observed at 722^o C.

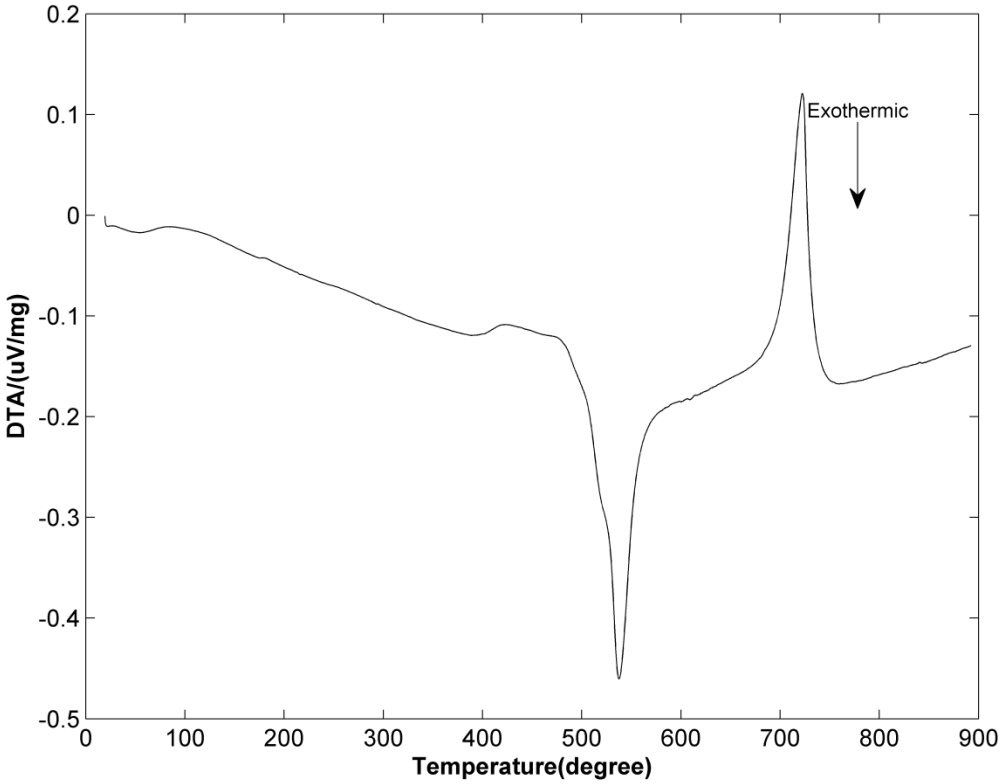

Figure I.1. Differential Thermal Analysis data.

Fig. I.2 shows the thermal expansion coefficient for bulk sample of phosphate based reactive glass. As the result indicates the thermal expansion is very small at low

www.manaraa.com

temperature and gradually increases up to 450 ^{o} C and then suddenly decreases. This phenomenon is due to the fact that the glass transitioning temperature is 469 ^{o} C and after that point the glass is usually releasing heat rather than absorbing. Also this is close to crystallization temperature where heat is actually released from the sample for structural change which explains the decrease in CTE value. Additionally CTE value for aforementioned temperature range is given in Table I.1.

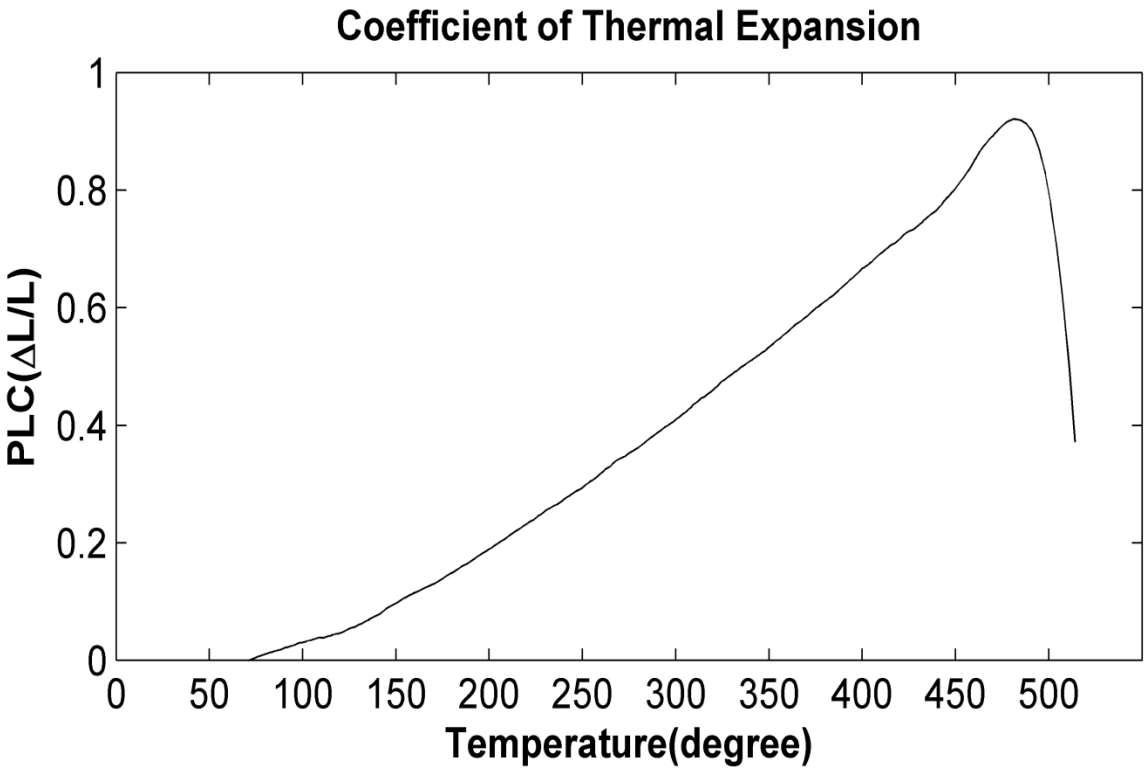

Figure I.2. Coefficient of Thermal Expansion.

www.manaraa.com

Table I.1. Coefficient of Thermal Expansion.

Temperature range (^{o}C)	Coefficient of Thermal Expansion (C^{-1})
71 ~ 100	1.04E-05
100 ~ 150	1.34E-05
150 ~ 200	1.84E-05
200 ~ 250	2.09E-05
250 ~ 300	2.32E-05
300 ~ 350	2.47E-05
350 ~ 400	2.67E-05
400 ~ 450	2.74E-05

Micro hardness results are shown in Fig. I.3 for different samples. The result indicates higher hardness at lower load value which is expected. But hardness drastically reduces with higher load and be saturated after 1.96 N until it reaches 4.96 N after which the load creates fracture in the sample so the results were not accepted. It is clear from the result that after 4.96 N load value this composition loss rigidity and fracture occurs.

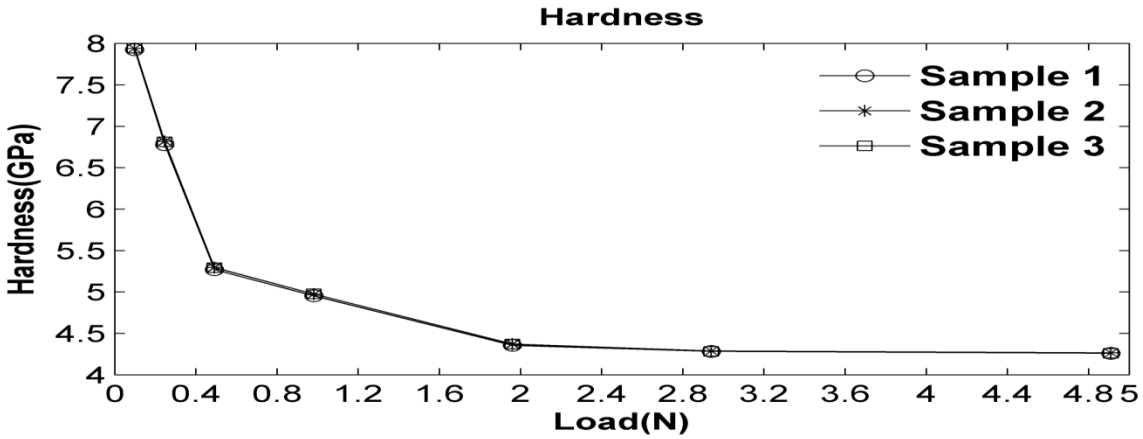

Figure I.3. Micro-hardness result.

www.manaraa.com

Surface region of optical fiber was analyzed before and after putting in the phosphate buffer solution. The results are shown below in Fig. I.4. The result shows the formation of a reaction layer after dissolution.

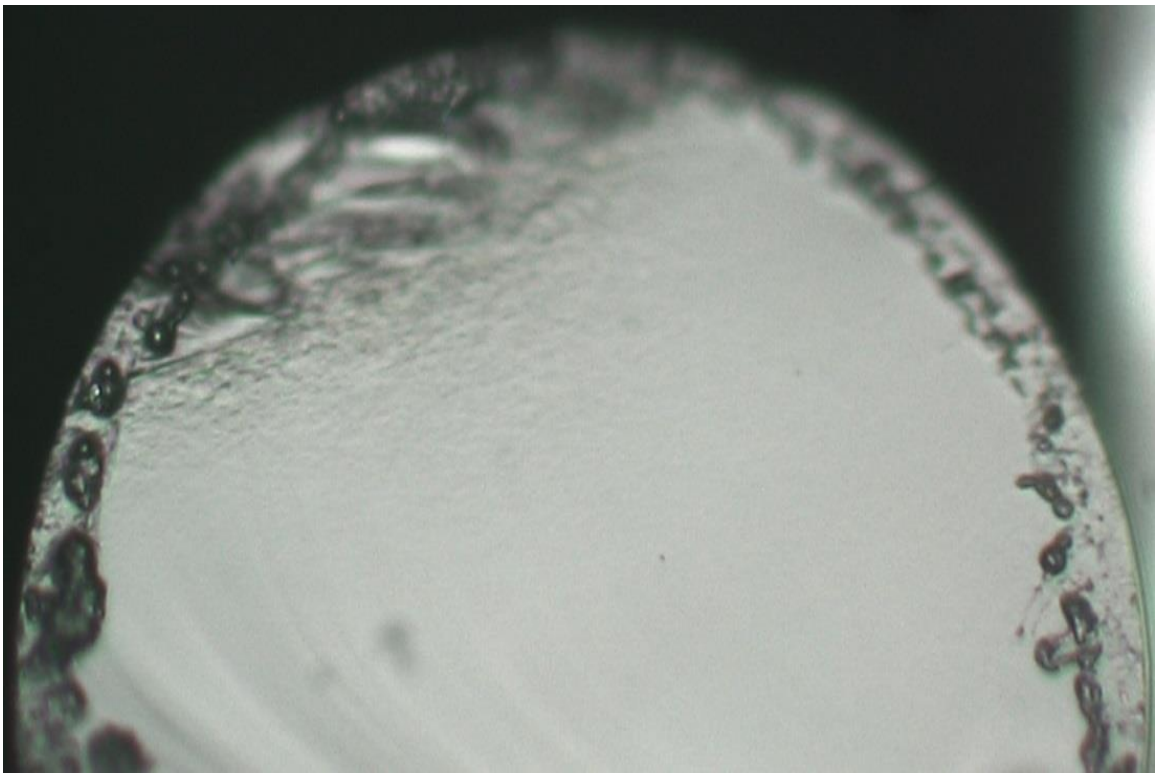

Figure I.4. Surface Analysis of phosphate fiber.

www.manaraa.com

VITA

Md Shihab Adnan was born in Dhaka, Bangladesh. He received his Bachelor of Science degree from Bangladesh University of Engineering and Technology, Dhaka, Bangladesh in Electrical and Electronics Engineering in 2011. He received his Master of Science in Electrical Engineering from Missouri University of Science and Technology in July 2016.

www.manaraa.com